

Journal of Geophysical Research: Solid Earth

RESEARCH ARTICLE

10.1002/2015JB012225

Key Points:

- GPS is used alone to realize a competitive terrestrial reference frame (TRF)
- This is enabled by new estimates of GPS satellite antenna phase variations
- GPS data from orbiters have an important impact on TRF and annual geocenter motion

Correspondence to:

B. J. Haines,

Bruce.J.Haines@jpl.nasa.gov

Citation:

Haines, B. J., Y. E. Bar-Sever, W. I. Bertiger, S. D. Desai, N. Harvey, A. E. Sibois, and J. P. Weiss (2015), Realizing a terrestrial reference frame using the Global Positioning System, *J. Geophys. Res. Solid Earth*, 120, 5911–5939, doi:10.1002/2015JB012225.

Received 19 MAY 2015

Accepted 22 JUN 2015

Accepted article online 14 JUL 2015

Published online 26 AUG 2015

Realizing a terrestrial reference frame using the Global Positioning System

Bruce J. Haines¹, Yoaz E. Bar-Sever¹, Willy I. Bertiger¹, Shailen D. Desai¹, Nate Harvey¹, Aurore E. Sibois¹, and Jan P. Weiss^{1,2}

¹Jet Propulsion Laboratory, California Institute of Technology, Pasadena, California, USA, ²Now at University Corporation for Atmospheric Research, Boulder, Colorado, USA

Abstract We describe a terrestrial reference frame (TRF) realization based on Global Positioning System (GPS) data alone. Our approach rests on a highly dynamic, long-arc (9 day) estimation strategy and on GPS satellite antenna calibrations derived from Gravity Recovery and Climate Experiment and TOPEX/Poseidon low Earth orbit receiver GPS data. Based on nearly 17 years of data (1997–2013), our solution for scale rate agrees with International Terrestrial Reference Frame (ITRF)2008 to 0.03 ppb yr⁻¹, and our solution for 3-D origin rate agrees with ITRF2008 to 0.4 mm yr⁻¹. Absolute scale differs by 1.1 ppb (7 mm at the Earth's surface) and 3-D origin by 8 mm. These differences lie within estimated error levels for the contemporary TRF.

1. Introduction

An accurate terrestrial reference frame (TRF)—as realized by the global network of space geodetic observatories—provides an important foundation for measuring changes in the shape of the solid Earth and its fluid envelope. In particular, successful monitoring of the long-term evolution of sea level, from both space (with radar altimeters) and the ground (with tide gauges), depends on a stable and accurate TRF [e.g., Morel and Willis, 2005; Beckley *et al.*, 2007; Blewitt *et al.*, 2010; Collilieux and Wöppelmann, 2011; Fu and Haines, 2013]. Driven in large measure by the demands of sea level monitoring, international initiatives are underway to improve the stability of the TRF to the 0.1 mm yr⁻¹ level [Plag and Pearlman, 2009; NRC, 2010; Merkowitz *et al.*, 2012]. This goal represents a factor-of-five improvement over the present state of the art [Wu *et al.*, 2011; Collilieux *et al.*, 2014].

The current standard for the most demanding scientific applications is designated the International Terrestrial Reference Frame (ITRF), updates for which are published regularly by the ITRF Center of the International Earth Rotation and Reference Systems Service (IERS) [Petit and Luzum, 2010; Altamimi *et al.*, 2011]. Each revision of the ITRF represents a practical, and thus imperfect, realization of an idealized International Terrestrial Reference System (ITRS). The origin and scale of this theoretical construct are physical: the former coincides with the center of mass (CM) of the whole Earth system, including its atmosphere and ocean, while the latter is defined by the SI meter. The overall system corotates with the Earth, and the orientation is equatorial but otherwise arbitrary and specified by international agreements. The initial orientation has maintained consistency with the Bureau International de l'Heure system at 1984.0 [Petit and Luzum, 2010]. The Z axis points in the direction of the mean pole (1984.0), and the X axis passes through the resulting equator near the Greenwich meridian. (The IERS reference meridian is approximately 100 m east of the Greenwich Meridian established by Sir George Airy in 1851 and represented by a brass strip at the Old Royal Observatory [Malys *et al.*, 2015].) The ITRS must somehow accommodate the continuous movements of the Earth's fragmented crust that are fueled by plate tectonics. The time evolution of the orientation is therefore defined by enforcing a no-net rotation condition for horizontal tectonic motions integrated over the Earth [cf. Chapter 4 from Petit and Luzum, 2010]. In realizing the TRF, these motions are treated as linear in time.

Advances in geodetic measurement techniques since the dawn of the space age are responsible for cultivating this notional ITRS. Indeed, space geodetic measurements provide the only viable means of accurately accessing the ITRS. The motions of artificial Earth-orbiting satellites are governed by laws of physics.

With underpinning from accurate tracking measurements linked to the Earth's crust, these laws provide natural constraints on geocenter and terrestrial scale. Also, enabling characterization of the terrestrial scale is the simultaneous observation of distant cosmic radio sources (quasars) from widely separated radio telescopes.

The origin of the ITRF has been traditionally realized by satellite laser ranging (SLR), while the scale has been derived from a combination of SLR and very long baseline interferometry (VLBI) [e.g., *Altamimi et al.*, 2011]. The contributions of GPS and Doppler Orbitography and Radiopositioning by Satellite (DORIS) to the ITRF are also critical. The corresponding ground networks are unrivaled in terms of their geographic diversity, and support refinement, and densification and dissemination of the frame. GPS sites are particularly abundant and play a crucial role in connecting the three other techniques [*Altamimi and Collilieux*, 2009]. Nearly all (82 of 84) of the ITRF2008 sites with technique colocations, for example, are represented by permanent GPS installations [*Altamimi et al.*, 2011]. There are nearly 600 total sites in ITRF2008, a large majority of which are occupied by Global Navigation Satellite System (GNSS) receivers tracking mainly GPS spacecraft, but also satellites from the Russian GNSS and other emerging systems (e.g., European Galileo).

The continuous 3-D observational diversity and high accuracy afforded by GPS, coupled with the considerable economic advantages of geodetic-quality GPS tracking systems, imply a prominent future role in advancing the TRF. Despite this promise, the capacity of GPS to define the fundamental parameters of the ITRF remains largely unrealized 37 years after the launch of the first GPS satellite in 1978. Lingering doubts about the absolute geocentric accuracy and independence of GPS at the millimeter to centimeter level have led to persistent exclusion of the data type from specification of the ITRF scale and origin [e.g., *Ray et al.*, 2004; *Altamimi and Collilieux*, 2009; *Collilieux et al.*, 2011]. These doubts are fed in part by fundamental weaknesses of the radiometric one-way GPS tracking observations, which imply clock errors must be dealt with through either differencing or explicit estimation. While this does not preclude the measurement of very accurate baselines (and thus scale), it can considerably weaken the ability of GPS to resolve the Earth CM relative to the global tracking network; estimation of pass-by-pass phase biases and tropospheric parameters further undermines the solution [*Kuang et al.*, 1996; *Rebischung et al.*, 2013]. When paired with the full (24–30 satellites) GPS constellation, however, the large ground network implies a remarkable network geometry that significantly compensates for the weaknesses of the fundamental GPS tracking observations [*Kuang et al.*, 2015]. We thus encounter many examples in the literature of successful applications of GPS for realizing the TRF.

Early studies predicted that GPS alone, with only a handful of ground stations, could support determination of the origin of the TRF at the few-centimeters level within 1 day [*Malla and Wu*, 1989]. While promising, the results from the first global GPS geodetic campaigns (Central and South America (CASA) Uno in 1988 and GPS IERS and Geodynamics Experiment (GIG) in 1991) were unable to bear out this prediction, due in part to the small number of GPS satellites and asymmetries of the primitive ground networks [*Vigue et al.*, 1992; *Blewitt et al.*, 1992; *Malla et al.*, 1993a]. With the establishment in 1992 of a permanent International GPS (now GNSS) Service (IGS) [*Beutler et al.*, 1999], TRF realization with GPS became increasingly routine. Accuracies improved with advances in GPS technologies and with the growth of both the ground and space segments. *Heflin et al.* [2002] developed an independent GPS-based frame that agreed with ITRF2000 to better than 1 cm and 1 ppb for origin (3-D) and scale, respectively. Based on over 10 years of GPS data, this frame definition also enabled evaluation of long-term stability: the 3-D origin drifted from ITRF2000 by 6 mm yr^{-1} and the scale by 0.1 ppb yr^{-1} (0.6 mm yr^{-1} at the Earth's surface).

As the original GPS constellation was gradually replenished with a new block of satellites beginning in 1997, the GPS-based scale estimates became increasingly unstable. This was attributed to mismodeling of the phase center locations of the GPS transmitter antennas [*Zhu et al.*, 2003]. It was widely recognized by this time that the manufacturers' estimates of the phase center locations of the complex GPS satellite navigation antennas were not appropriate for the most demanding geodetic applications [e.g., *Bar-Sever*, 1998; *Mader and Czopek*, 2002; *Schmid and Rothacher*, 2003]. The impact on the TRF recoveries, however, was not fully appreciated until a cluster of GPS replenishment satellites was launched in 2000, rapidly altering the composition of the constellation. This exposed important differences in the scale stability linked to differing conventions for modeling of the antenna phase centers [*Ge et al.*, 2005].

With the support of new standards for modeling of the satellite antenna phase centers and variations, GPS can now provide competitive levels of accuracy for realization of the scale and origin of the TRF [*Rüelke et al.*, 2008; *Desai et al.*, 2011; *Argus*, 2012]. Recent reprocessed GPS network solutions (spanning 1996–2009) realize the origin to within 1 cm and 1 mm yr^{-1} of ITRF2008 for bias and rate, respectively [*Collilieux et al.*, 2011].

These GPS realizations, however, are not fully independent: the models for the transmitter antennas are developed from ground tracking data, wherein the station locations are fixed to values from the prevailing ITRF [Schmid *et al.*, 2005]. This implies that the GPS-derived terrestrial scale, in particular, is inherited from the ITRF and thus dependent on VLBI and SLR [e.g., Ray *et al.*, 2004; Rülke *et al.*, 2008; Collilieux *et al.*, 2011].

Our goal is to realize a competitive TRF which is independent of any a priori frame definition, based on GPS data, physical constants (primarily GM and low-order gravity terms), equipment specifications, and nothing else. We hope this will provide new insights on limiting error sources and also inform decisions on the contribution of GPS in multitechnique frame realizations. A main element of our strategy is the use of GPS data collected in low Earth orbit—treating the host satellite as an orbiting fiducial laboratory—either to provide independent estimates of the transmitter antenna phase variations [e.g., Haines *et al.*, 2004, 2005] or to supplement terrestrial stations in network solutions [e.g., Haines *et al.*, 2011; Weiss *et al.*, 2013; Kuang *et al.*, 2015]. We note that the plans behind the proposed NASA Geodetic Reference Antenna in Space (GRASP) mission [Nerem *et al.*, 2011] follow a similar blueprint. Our approach also rests on a long-arc (9 day) network solution strategy that is tailored to reference frame realization and designed to better overcome some of the inherent weaknesses of the GPS observations. We describe these elements in greater detail below, beginning with the antenna models that provide the foundation for the TRF estimates.

2. GPS Transmit Antennas

When several radionavigation concepts coalesced into GPS in the 1970s, the potential of the system to advance geodesy was already being probed [Anderle, 1978; MacDoran, 1979; Counselman and Shapiro, 1979]. It could not have been anticipated, however, that the system might eventually support millimeter-level geodetic measurements at global scales. At this level of accuracy, detailed characterizations of the space systems (e.g., attitude behavior, bus and solar panel material properties, and antenna patterns) are crucial. Much of this information is unavailable from traditional sources because the requirements on the GPS measurement systems were driven by the demands of navigation rather than geodesy.

Despite the challenges posed by complex spacecraft forms and uncertain details in attitude variation models, advances in precise orbit determination (POD) have enabled 2–3 cm accuracies (3-D 1σ) for postprocessed GPS ephemerides [Griffiths and Ray, 2009; Steigenberger *et al.*, 2009]. Due to the dynamical nature of the POD process, these accuracy figures pertain to the location of the spacecraft CM in the geocentric frame. As with any space-based geodetic technique, these precise orbit solutions provide the framework for making accurate measurements of the deforming Earth.

Unfortunately, the accuracy of the GPS satellite ephemerides has not been fully exploited in global geodetic applications, such as TRF realization. One limiting factor is the uncertainty in locating the effective radiating point for the GPS transmissions from each vehicle [Zhu *et al.*, 2003]. To best reconcile GPS observations with the integrated vehicle path, the local vector between the spacecraft CM and the electrical phase center of the transmit antenna should be accurately modeled. While the magnitude of this vector is on the order of only 1 m, it is not straightforward to measure. The main difficulty lies not with the measurement of the CM in the spacecraft frame. (Prelaunch measurements for several Block IIA spacecraft, for example, agreed at the 6 mm level [Mader and Czopek, 2001].) Rather, the challenge rests in measuring the offset (location) of the antenna phase center (APC) with respect to the spacecraft CM and the variations (antenna phase variations, APV) about this offset.

Signals radiating from the transmit antenna cannot be ascribed to a single source location. Group delay (pseudorange) measurements are associated with a different effective radiating point than phase measurements, and both will experience important variations with line of sight to the receiver. These line-of-sight variations are due not only to the gain pattern of the transmitting antennas [Aparicio *et al.*, 1996] but also to spacecraft multipath [Young *et al.*, 1985]. The situation for GPS satellites is exacerbated by the complex design of the navigation antennas, which feature 12 helical elements arranged in two concentric rings (Figure 1).

Fortunately, errors in locating the GPS APCs in the spacecraft frame are not fully expressed in geolocation. Owing to the differential nature of the GPS tracking technique, there is significant cancellation of APC errors. A spurious 1 m shift of all the GPS spacecraft APC locations in the nadir direction induces a scale error at the



Figure 1. (left) GPS (Block II) satellite antenna panel, showing the two concentric rings of helical antenna elements mounted on a ground plane. The inner ring of four elements supplies 90% of the total power at the L band. The remaining power is allocated to the outer ring of eight elements, which broadcasts 180° out of phase with respect to the inner ring [Mader and Czopek, 2001]. (right) A typical GPS terrestrial receiver antenna for geodetic applications, which features a Dorne Margolin antenna element mounted on a choke ring ground plane. Inspired by the GPS antenna for the TOPEX/Poseidon satellite [Tranquilla and Colpitts, 1989], the choke ring design suppresses significant low-angle multipath [Young et al., 1988; Tranquilla et al., 1994]. In contrast to the GPS satellite antennas, the ground antenna is compact (0.4 m diameter) and its electromagnetic properties have been extensively measured and published.

Earth's surface of only 5 cm [Springer, 2000; Zhu et al., 2003]. Most of the APC error is removed by differencing measurements between ground stations or absorbed in the solutions for the clock offsets (in undifferenced GPS techniques).

Nonetheless, uncertainty in the GPS transmit APC remains a limiting source of error in GPS-based global geodesy. Ge et al. [2005] demonstrated that errors in contemporaneous international (IGS) standards for the GPS APC induced a rapid scale change of about 1 ppb over 1 year. They attributed this effect to the evolution of the GPS space segment: as legacy satellites were gradually replenished with modernized systems, the ensemble effect of the APC errors on the different satellite types (blocks) changed. Numerical simulations by Cardellach et al. [2007] suggested that APC mismodeling led to vertical network distortions of 6–12 mm and geographically correlated errors in the vertical rate of 1–2 mm yr⁻¹. Errors at this level significantly distort measurements of sea level change and carry important consequences for any studies which demand accurate (few mm and tenths of mm yr⁻¹) measurements of vertical crustal deformation. Accordingly, significant attention has been devoted to improved modeling of the GPS transmit antenna phase centers and variations. Some of these efforts have focused on ground calibration of the GPS satellite antenna panel shown in Figure 1 [Mader and Czopek, 2001, 2002; Wübbena et al., 2007], while others have used on-orbit data [e.g., Bar-Sever, 1998; Schmid and Rothacher, 2003; Schmid et al., 2005; Haines et al., 2005]. Regardless of the approach, the main focus has been on calibrating the antennas for the dual-frequency (ionosphere-free) combination of the GPS carrier phase ($\text{LC} \approx 2.54(\text{L1}) - 1.54(\text{L2})$). Unless noted otherwise, all results in this paper refer to this linear data combination, which provides the basis for global geodesy from GPS.

2.1. Using Terrestrial Antennas as References

The current IGS standards for GPS satellite antenna phase center offsets and variations are based on the precise evaluation of GPS on-orbit data as received by a global ground network. In contrast to the large, complex satellite (transmit) antennas, the ground (receive) antennas are compact and designed with geodetic applications in mind (Figure 1). A number of agencies and antenna manufacturers have expended significant effort on calibrating various ground antenna and radome combinations represented in the global IGS network [Schmid, 2012]. These calibrations are based on either a robotic field technique [Wübbena et al., 2000] or relative field calibrations [Mader, 1999]. It should be noted, however, that the intrinsic APV patterns of the antenna/radome pairings in isolation can be significantly altered by near-field effects (multipath and scattering) unique to each terrestrial tracking site. As highlighted by Elósegui et al. [1995], the permanent structures (e.g., pillars) to which the antennas are typically mounted become electromagnetically coupled

to the antennas themselves. Calibration systems for recovering the comprehensive site-dependent antenna patterns (intrinsic APV plus multipath) have yielded promising results [Park *et al.*, 2004; Wübbena *et al.*, 2006]. These hardware systems, however, involve the use of large high-gain antennas or robots and have not yet been widely used to provide site-specific antenna calibrations, e.g., for a globally dispersed network of GPS ground stations.

To recover the GPS satellite antenna patterns for the current IGS standards, the calibrations for the terrestrial antennas are fixed in the network solutions. In order to overcome a near singularity in the solution, the scale of the ground network must also be fixed (e.g., to the value determined from SLR/VLBI as manifest in the current ITRF) [Springer, 2000]. If a sufficiently large number of globally dispersed stations are used, Schmid *et al.* [2005] reason that local effects such as multipath and unmodeled troposphere variation should have only minor influence on the results.

2.2. Using Orbiting Antennas as References

In this paper, our strategy for recovering the antenna phase center and variations of the GPS transmitters uses data from geodetic-quality GPS receivers in low Earth orbit (LEO). This approach offers a number of substantial advantages. Most importantly, POD techniques can be invoked to estimate the average distance between the centers of mass of the Earth and receiving satellite with centimeter-level accuracy, and with negligible sensitivity to the scale of the TRF. This gravitational constraint on scale is central to all satellite geodetic techniques and stems from the ability of modern tracking systems to measure orbital periods (P) with microsecond-level accuracy [Born *et al.*, 1986]. It follows from Kepler's third law that few-millimeter accuracy can in theory be achieved for the semimajor axis, a , which is analogous to the average height of the satellite over a revolution. In the context of this simplified two-body problem, the limiting error source in determining a is the uncertainty in the geocentric gravitational constant, GM , which is the proportionality constant (i.e., $a^3 = (0.25 \times GM \times \pi^{-2})P^2$). GM is known to an accuracy of one half of a part per billion (ppb) from satellite laser ranging (SLR) [Dunn *et al.*, 1999; Ries and Cheng, 2014], which corresponds to errors in a of 1 and 4 mm, respectively, for the 1000 and 20,000 km altitudes of LEO and GPS satellites [cf. Zhu *et al.*, 2003]. Accurate measurement of the orbital period is also contingent on the knowledge of the Earth's orientation, which is required to align the TRF (linked to tracking stations on the crust) to the celestial frame (in which the equations of motion are described). Contemporary bulletins of length of day, for example, are accurate to $10\text{--}15 \mu\text{s d}^{-1}$ [Gambis and Luzum, 2011]. It is straightforward to confirm from Kepler's third law (above) that an error of $10 \mu\text{s}$ in measuring the 12h GPS orbital period (P) would induce an error of only 4 mm in the mean height (a) of the GPS orbits.

In practice, inadequate modeling of nonconservative forces (e.g., solar radiation pressure, albedo, anisotropic thermal reradiation, and antenna thrust) limits the accuracy that can be achieved for the time-averaged height (a) of the satellite. Even for the large, complex GPS satellites, however, modeling errors are not expected to impact a by more than 1–2 cm [Ziebart *et al.*, 2005].

When using LEO data to calibrate the GPS transmitters, this important gravitational constraint is now accessible to both the transmitter (GPS satellite) and the receiver (LEO satellite). In contrast, antenna calibrations that rely on terrestrial GPS tracking data [e.g., Bar-Sever, 1998; Schmid and Rothacher, 2003; Schmid *et al.*, 2005] can access this gravitational constraint only on the transmitter side, since ground receivers are not in free fall. Additional information on this important gravitational constraint and its implications on our conclusions can be found in the Appendix.

Another advantage of relying on orbiting antennas is that there is no troposphere refraction to confound interpretation of the measurements. The only significant atmospheric refraction arises from the presence of free electrons in the ionosphere above the low orbiter carrying the GPS antenna. Since the ionosphere is a dispersive medium, the resulting signal delay is corrected to first order using the two GPS frequencies. Thus, in contrast to terrestrial GPS applications, no additional modeling or estimation of atmospheric delays is needed.

Haines *et al.* [2004] combined GPS data from the Jason-1 [Ménard *et al.*, 2004] and Gravity Recovery and Climate Experiment (GRACE) [Tapley *et al.*, 2004] missions to solve for the antenna phase and group-delay variations (ionosphere free) for each of the GPS satellites flying in the 2002–2004 time frame. These ad hoc calibrations were designed to improve the Jason-1 orbit solutions and did not yield estimates of the phase center offsets of the GPS transmitters. However, application of these GPS transmitter antenna calibrations did consistently improve the RMS fits to independent tracking data from ground stations, albeit by a small amount (0.05 to 0.10 mm for ionosphere-free phase). The calibrations also showed important azimuthal variations in the APV

pattern, which faithfully depicted known positions of individual helical elements of the GPS satellite antenna panel [cf. *Haines et al.*, 2004, Figure 3]. Similar azimuthal patterns have also been identified in the processing of ground data [e.g., *Schmid et al.*, 2005; *Dilssner*, 2010] but are not yet part of the IGS standard. The IGS, however, has standardized the use of LEO-based extensions to the APV calibrations for the GPS satellites [*Jäggi et al.*, 2013]. These extensions are aimed at providing antenna phase characteristics at high nadir angles ($>14^\circ$), so they can be used to support GPS-based POD of low Earth orbiters. For the portions of the beam ($<14^\circ$) that illuminate the Earth, however, the IGS standard calibrations are still based on terrestrial data.

In a series of abstracts, we have described several evolutions to our LEO-based antenna calibrations. Early GRACE-based calibrations of the GPS transmitters practically eliminated a long-unexplained error in the realization of GPS measurements from the TOPEX/Poseidon (T/P) altimeter mission. In particular, a 6 cm anomaly in the solved-for height of the T/P GPS antenna boom [*Bertiger et al.*, 1994] was reduced to insignificance [*Haines et al.*, 2006]. Similar GRACE-based calibrations significantly stabilized the scale of the TRF realized from GPS alone [*Haines et al.*, 2007], while updated LEO-based antenna calibrations have shown promise for determining the complete TRF, including the origin as well as scale [e.g., *Haines et al.*, 2007; *Desai et al.*, 2008; *Haines et al.*, 2011; *Weiss et al.*, 2013]. To provide the basis for realizing the TRF in the present study, we use GPS data from the GRACE and T/P satellites to develop a new set of comprehensive calibrations for both phase and group delay variations of the GPS satellites.

2.3. Antenna Phase Variations From TOPEX/Poseidon and GRACE

Launched in 1992, the TOPEX/Poseidon (T/P) satellite featured a pioneering GPS Demonstration Receiver (GPSDR) tracking from a choke ring antenna assembly mounted on a 4 m boom (Figure 2). Data from the GPS system on T/P supported radial RMS orbit accuracies better than 3 cm soon after launch [*Bertiger et al.*, 1994]. The GPSDR did not use codeless tracking techniques, and the most accurate (ionosphere-free) observables could be formed only when the GPS antispoofing (AS) function was turned off. For the purposes of antenna calibration, most of the useful T/P data were thus collected prior to the 31 January 1994 implementation of AS on the GPS constellation.

Despite the limitations imposed by the nascent ground network and GPS constellation, the T/P data set represents an indispensable resource for the calibration of the GPS transmit antennas. The position of the choke ring assembly away from the bus minimized near-field phase multipath from the spacecraft, reducing corruption of the transmitter APC and APV estimates. Also important, the 1330 km altitude of the mission enables characterization of the transmitter APV at high nadir angles (between 14° and 17°) inaccessible from the ground but relevant to space applications of GPS.

The GRACE mission is comprised of twin satellites occupying a \sim 500 km altitude, near-polar (89.5° inclination) orbit [*Tapley et al.*, 2004]. One of the twins trails the other by 170–220 km along the satellites' track. Both carry advanced, codeless BlackJack GPS receivers connected to choke ring antennas embedded on the top of the spacecraft bus (Figure 2). The clean spacecraft form is desirable from a multipath standpoint, but important near-field effects are still expected. In contrast to T/P, however, the GRACE missions have collected years of accurate dual-frequency tracking measurements against the backdrop of a mature GPS constellation and ground network.

To support calibration of the GPS satellite antennas, we generated customized daily POD solutions for both T/P and GRACE using the Jet Propulsion Laboratory (JPL) GPS Inferred Positioning System/Orbit Analysis and Simulation II (GOA) software (<http://gipsy.jpl.nasa.gov>). The T/P solutions cover 1993, while the GRACE solutions span 2002–2012. We considered only data from GRACE-B in order to avoid occasional contamination of the GRACE-A tracking data due to interference from a side-looking GPS occultation antenna. To preserve the link between scale and gravity, we adopt dynamical POD strategies for both T/P and GRACE-B, details of which are provided in Tables 1 and 2, respectively.

Out of an abundance of caution, we use fiducial-free GPS satellite orbit and clock products [*Hefflin et al.*, 1992] to provide the framework for the POD in order to avoid any dependence on prior TRF realizations. In most cases, these are legacy products from JPL, predating the introduction of the ground-based transmitter APV calibrations. (For the legacy products, the basis for the transmitter APC offsets is a prelaunch theoretical estimate from the manufacturer of the Block II/IIA GPS satellites [*Love*, 1984; *Mader and Czopek*, 2002]. This theoretical value was fixed by *Bar-Sever* [1998] in solving for the APC offset of the IIR replenishment satellites.) For

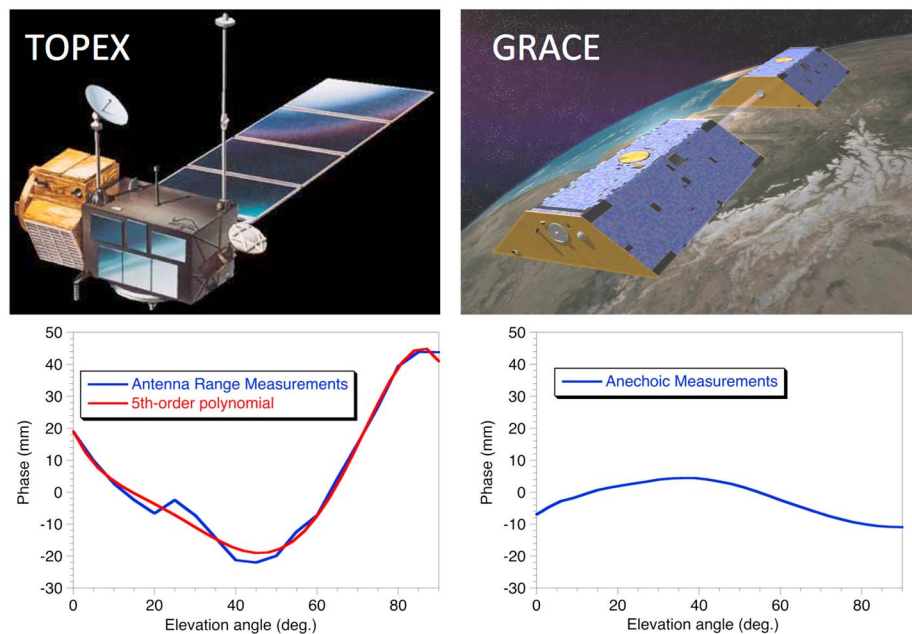


Figure 2. Antenna phase variation (APV) as a function of elevation angle for the (left) TOPEX and (right) GRACE antennas, respectively. In both cases, the APV is for the ionosphere-free carrier phase (LC) and corresponds to the incremental delay with respect to a best fit antenna phase center (APC). The TOPEX antenna consists of a helical element (L. Young, private communication, 2010) mounted on choke ring ground plane [Tranquilla et al., 1994]. The APV of the antenna assembly was measured at an outdoor antenna range [Young et al., 1993]. For this study, the elevation variations were smoothed using a fifth-order polynomial fit (shown). The GRACE antennas consist of dual-frequency patch elements mounted on smaller choke ring ground planes. The GRACE antenna phase properties were measured in an anechoic chamber [Purcell, 1999a, 1999b]. The APV patterns in both the TOPEX and GRACE cases describe the behavior of the antenna assembly in isolation. Multipath mitigation, however, was a key factor in the design of each of the GPS subsystems: the TOPEX GPS antenna was mounted on the top of a 4 m boom, and the GRACE antenna was embedded on the top surface of a simple, clean spacecraft exterior.

the earliest (1993) and most recent (2009–2012) time periods, the legacy JPL products are either of uneven quality or unavailable (having been retired in 2009). In these cases, we use experimental (fiducial-free) GPS orbit and clock products based on prior generations of our LEO-based antenna calibrations.

Our goal is not to generate the most accurate T/P and GRACE orbit solutions possible, but rather to build a stable framework for antenna calibrations, buttressed by the gravitational constraint to the extent possible rather than any definition of the TRF. This antenna calibration also requires a priori models of the two LEO antennas, which serve as our candidate reference antennas in space. For both T/P and GRACE-B, the models are based on prelaunch measurements of the phase variations of the choke ring antenna assemblies in isolation, i.e., not mounted on the vehicle or a mock-up of the vehicle. The a priori phase pattern for the T/P choke ring antenna came from outdoor antenna test range measurements collected at JPL [Young et al., 1993]. To reduce suspected test range errors, we averaged the T/P APV by elevation and smoothed the resulting elevation dependence using a fifth-order polynomial (Figure 2). The a priori phase pattern of the GRACE antenna is from anechoic chamber measurements [Purcell, 1999a, 1999b]. In contrast to T/P, the GRACE a priori model used in this study includes the complete pattern, including azimuthal variations.

As part of the daily POD computations, the partial derivatives of both the transmitter and receiver APVs are computed and retained in normal equations produced by the GOA filter. These daily normal equations are combined across both missions, applying constraints to recover the transmitter APV as a function of the GPS satellite antenna type: (1) Block II/IIA (satellites launched between 1989 and 1997), (2) Block IIR-A (replenishment satellites with legacy antenna panels, launched between 1997 and 2003), (3) Block IIR-B/M (replenishment satellites with upgraded antenna panels, launched between 2003 and 2009), and (4) Block IIF (follow-on satellites, launched from 2010 to present). Block II/IIA satellites were observed by both T/P (in 1993) and GRACE (2002–), providing a means of projecting T/P-based calibrations onto modernized GPS satellites. While there is evidence for differences among the APC offsets for satellites within each block [Schmid et al., 2005],

Table 1. GRACE Precise Orbit Determination Strategy

Background Model	Source/Value	Reference
GRACE s/c properties		<i>Bettadpur</i> [2012]
Mass	487.2 kg	
Surface areas	Macro model	
Thermal properties	Macro model	
GRACE attitude	Quaternions	
GPS receive antenna		
Gr-A CM to APC (mm)	(−0.400, −0.400, −413.967)	<i>Bettadpur</i> [2012]
Gr-B CM to APC (mm)	(+0.602, −0.754, −414.277)	<i>Bettadpur</i> [2012]
Antenna phase variations	Anechoic	<i>Purcell</i> [1999a, 1999b]
Static geopotential field	GGM02C (200 × 200)	<i>Tapley et al.</i> [2005]
Ocean tide potential	FES2004	<i>Lyard et al.</i> [2006]
Solid tide potential	IERS2010	<i>Petit and Luzum</i> [2010]
Third-body potential	DE405	<i>Standish</i> [1998]
Atmospheric density	DTM94	<i>Berger et al.</i> [1998]
Solar radiation pressure	JPL (Earth/Moon shadow)	
Earth radiation pressure	UT Albedo + IR	<i>Knoche</i> [1989]
GPS s/c orbits	JPL fiducial free	See text
GPS s/c clock offsets	JPL fiducial free	See text
Estimated Parameter	Parameterization	σ
Epoch state		σ_p
Position (x_o, y_o, z_o)		100 km
Velocity ($\dot{x}_o, \dot{y}_o, \dot{z}_o$)		1 km s ^{−1}
Clock offset	White noise: 5 min updates	1 s
Carrier phase biases	White noise update at breaks <i>Dynamic Iteration</i>	3 × 10 ⁵ km
Drag coefficient (C_D)	Bias	100
Empirical accelerations (cos, sin)		—
1/rev cross track	Bias	0.1 m s ^{−2}
1/rev along track	Bias	0.1 m s ^{−2}
1, 2, 3 d ^{−1} along track	Bias	1 mm s ^{−2}
		—
		Reduced-Dynamic Iteration
Drag coefficient (C_D)	White noise: 1/rev updates	100
Empirical accelerations (cos, sin)		100
1/rev cross track	White noise: 1/rev updates	10 nm s ^{−2}
1/rev along track	White noise: 1/rev updates	50 nm s ^{−2}
Tracking Data	σ	Rate
Ionosphere-free carrier phase: LC = 2.54(L1) − 1.54(L2)	1 cm	5 min

prior analysis suggests that block-averaged phase patterns (APC + APV) are sufficiently representative to support stable realization of the TRF [e.g., *Haines et al.*, 2010]. To compensate for the variations in the tracking data density in angular area units, we use variable-size azimuthal bins to describe the transmitter APV in the estimation process. To provide a manageable parameterization for application of the APV estimates, we subsequently interpolate the estimates to regular grid intervals: 2° × 1° and 2° × 3° in azimuth and elevation for the transmitter and receiver, respectively.

Recovered simultaneously in the filtering process are estimates of residual APV (with respect to a priori) for the LEO antennas (T/P and GRACE). Similarly parameterized, these estimates are expected to capture LEO spacecraft (s/c) phase multipath not represented in the prelaunch antenna calibrations. We applied certain

Table 2. TOPEX/Poseidon Precise Orbit Determination Strategy

Background Model	Source/Value	Reference
TOPEX s/c properties		
Mass	2406.433 kg	
Surface areas	Macro model	Marshall and Luthcke [1994]
Optical/thermal coefficients	Macro model	Marshall and Luthcke [1994]
TOPEX attitude	Nominal law (event file)	
GPS receive antenna		
CM to APC (xyz, mm)	(1949.4, 40.9, -4581.6)	
Antenna phase variations	JPL test range	Young et al. [1993]
Static geopotential field	GGM02C (200 × 200)	Tapley et al. [2005]
Ocean tide potential	CSR4.0	Eanes and Bettadpur [1996]
Solid tide potential	IERS2010	Petit and Luzum [2010]
Third-body potential	DE405	Standish [1998]
Atmospheric density	DTM2000	Bruinsma et al. [2003]
Solar radiation pressure	JPL (Earth/Moon shadow)	
Earth radiation pressure	UT Albedo + IR	Knoche [1989]
GPS s/c orbits	JPL fiducial free	See text
GPS s/c clock offsets	JPL fiducial free	See text
Estimated Parameter	Parameterization	σ
Epoch state		σ_p
Position (x_o, y_o, z_o)		100 km
Velocity ($\dot{x}_o, \dot{y}_o, \dot{z}_o$)		1 km s ⁻¹
Clock offset	White noise: 5 min updates	1 s
Carrier phase biases	White noise update at breaks	3 × 10 ⁵ km
Drag coefficient (C_D)	Bias	1000
Empirical accelerations (cos, sin)		
1/rev cross track	Bias	0.1 m s ⁻²
1/rev along track	Bias	0.1 m s ⁻²
Tracking Data		Rate
Ionosphere-free carrier phase: LC = 2.54(L1) - 1.54(L2)		1 cm
		5 min

constraints to overcome strong correlations between the elevation angle, as viewed from the receiver, and the nadir angle, as viewed from the transmitter.

When treating T/P as reference, we fixed the elevation dependence of the receiver antenna to the a priori (smoothed test range) model (Figure 2) but solved for the azimuthal variations. This constraint is based on the assumption that the mean elevation-dependent signature of T/P multipath, when averaged over long periods of time, is small. Using simulation tools prior to T/P launch, Hajj [1989] found mainly short-period (~1 min) phase multipath associated with reflections from another elevated antenna (Tracking and Data Relay Satellite System) and the solar panel. He projected the multipath signal would be significantly (~20 dB) weaker than the direct signal, due mainly to the placement of the antenna on a 4 m boom. He also cautioned that the multipath interference would be considerably greater if the T/P GPS antenna were mounted on the bus surface, which is exactly the configuration used by the GRACE mission (Figure 2).

Figure 3 (left) shows the projected phase multipath for the GRACE mission, based on a more recent version of the same simulation tool set [Byun et al., 2002]. For this particular simulation, the spacecraft surfaces are assumed to be perfect conductors, implying that the amplitude of the real variations may be lower by a constant (scale) factor. The predicted multipath error nonetheless shows important systematic effects, particularly at low to middle elevations as viewed from GRACE. In relative terms, the multipath signal at high elevations is much weaker. We chose our constraints accordingly: along two high-elevation azimuthal cuts (shown) with

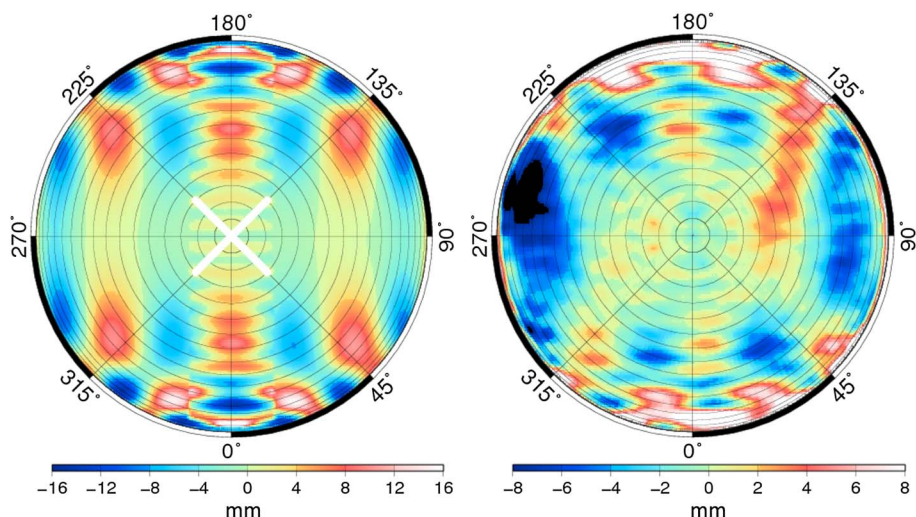


Figure 3. (left) Predicted and (right) estimated GRACE multipath for the GPS ionosphere-free carrier phase (LC) as a function of azimuth (0° – 360°) and elevation (90° – 0°) in the s/c frame. Based on the software tool described by *Byun et al.* [2002], the simulation assumes that the s/c surfaces are perfect conductors and is intended to capture the patterns, but not necessarily the correct amplitude, of the multipath signal. The white cross in the center of the plot depicts the constraint used in the estimation of the transmitter and receiver APVs. This cross spans regions of weak multipath and defines two azimuthal transects ($>60^\circ$ elevation) where the GRACE APV is constrained to match the intrinsic APV of the antenna in isolation (as measured in an anechoic chamber). Shown in the right panel is the estimated multipath signal, which is recovered simultaneously with the GPS block-specific transmitter APVs. In view of the difficulty in simulating details of the multipath contamination, the agreement between the predicted and recovered multipath is considered a favorable indicator for the overall APV estimation process.

weak predicted multipath, the GRACE APV is forced to match the a priori (anechoic) calibration. While this constraint is much weaker than the comparable choice for T/P, our results suggest that it is sufficient, when used with the decade-long GRACE-B data set, to separate the transmitter and receiver APV.

The partial derivatives for the APV assume a locally bilinear form, which constrains estimates from neighboring bins. Slight variations in the receiver/transmitter geometry are experienced as the participating satellites (GPS and GRACE) trace out their eccentric orbits, and also perhaps due to small variations in pointing. Accumulated over years, these variations appear to be enough to randomize the local mapping between receiver and transmitter elevation bins. Together with the bilinear constraint, this randomization provides some means of separating the transmitter and receiver APV. At the same time, this interplay leads to overoptimistic estimates of formal error and will, at some level, yield systematic errors. Results from GRACE are at least reasonably consistent: dividing the data set into two distinct 4 year periods (early and late missions) and applying the same constraint lead to similar results, i.e., 3 mm level agreement for the corresponding transmitter APV estimates.

Reassuringly, if we apply the same (stronger) elevation constraint used in the T/P case, the resulting transmitter APV estimates differ by only 1–2 mm (1σ) from the comparable estimates generated in the presence of the (weaker) high-elevation constraints. Even though the differences are small, we prefer an approach which recognizes the stronger multipath on GRACE (versus T/P) and attempts to minimize contamination of the transmitter APV by this source. The estimated multipath for GRACE is depicted in the right panel of Figure 3 and shows the same general arrangement of patterns predicted by the simulation tool, but with (2x) smaller amplitudes. In view of the challenges posed by multipath modeling, this level of agreement is encouraging.

Figure 4 shows the nadir angle dependence of the recovered GPS transmitter APV_{CM} using T/P and GRACE-B, respectively, as reference. (We use the subscript CM here to denote that the datum for the APV is the space-craft center of mass. Reflected in APV_{CM} are both the phase center offset and variations about the offset.) For comparison, we provide comparable values for the current (IGS08_1793) standard, which is based on reduction of GPS data from the global ground network [e.g., *Schmid et al.*, 2005]. Also shown (for the Block II/Ia antenna only) are the values from the outdoor robot calibration [*Wübbena et al.*, 2007] of the GPS antenna panel pictured in Figure 1. To construct this curve, we began with the data underlying the elevation angle variation shown in Figure 7 of *Wübbena et al.* [2007] and superimposed the total offset to the spacecraft

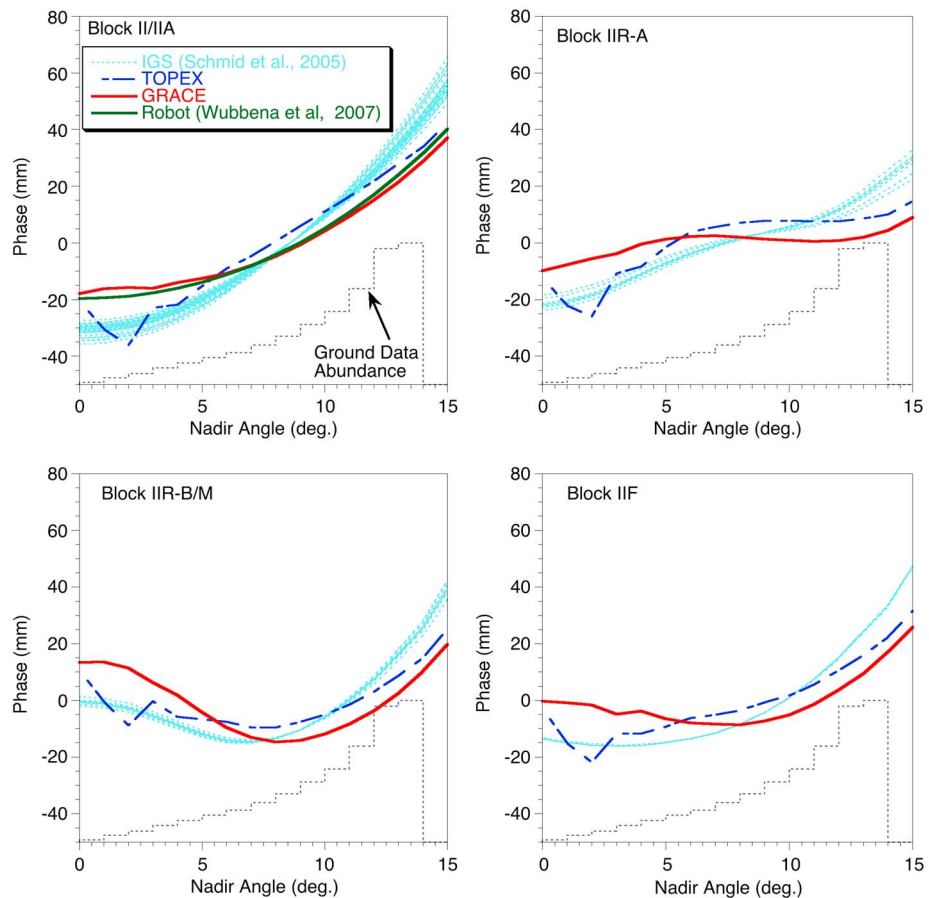


Figure 4. GPS transmitter antenna phase variations (APV_{CM}) as a function of nadir angle for the four current antenna types. In all cases, the APV_{CM} is for the ionosphere-free carrier phase (LC) and corresponds to the total delay with respect to the spacecraft center of mass (CM). The blue and red lines show block-averaged estimates derived from LEO data using TOPEX/Poseidon and GRACE as the reference antenna, respectively. The light blues lines depict the current International GNSS Service standards (IGS08_1793), which are satellite specific and based on the reduction of terrestrial data [Schmid *et al.*, 2005]. The green line (Block II/IIA only) shows measurements from the robot calibration technique [Wübbena *et al.*, 2007]. The normalized distribution of tracking data from a typical ground network is depicted by the gray, hashed line and illustrates the increasing abundance of data with increasing nadir angle until the Earth's limb is reached at $\sim 14^\circ$.

CM (1693 mm). The latter is the sum of the estimated APC offset from the top of the ground plane (975 mm from Wübbena *et al.* [2007]) and the vertical offset of the ground plane from the CM (718 mm from Mader and Czopek [2002]).

While the differences between the GRACE- and T/P-based estimates (Figure 4) are not fully understood, they are in keeping with the error budget ($\sim 1 \text{ cm LC}$) for the T/P test range antenna calibration undertaken in Spring 1992 [Young *et al.*, 1993]. (The uncertainty in the anechoic measurements of the GRACE antenna is closer to 1 mm [Purcell, 1999b], about an order of magnitude smaller.) Residual multipath on both GRACE and T/P—imperfectly accommodated in our estimation procedure—may also contribute.

Noteworthy in Figure 4 is the steeper APV_{CM} for the IGS standard calibrations in comparison to the LEO- and robot-based estimates. One possible explanation is contamination of the IGS estimates by near-field multipath that does not average down globally, due for example to prevailing practices for antenna placement and associated monumentation. Surfaces near the antenna can be the source of important reflected signals, which will always arrive after the direct signals. Uncertainties in the LEO and robot techniques undoubtedly also play some role in explaining the differences observed in Figure 4.

What is most striking in Figure 4, however, is the close agreement between the GRACE- and robot-based results from the Block II/IIA antenna. The APV_{CM} estimates as a function of nadir angle agree to 2 mm (1σ),

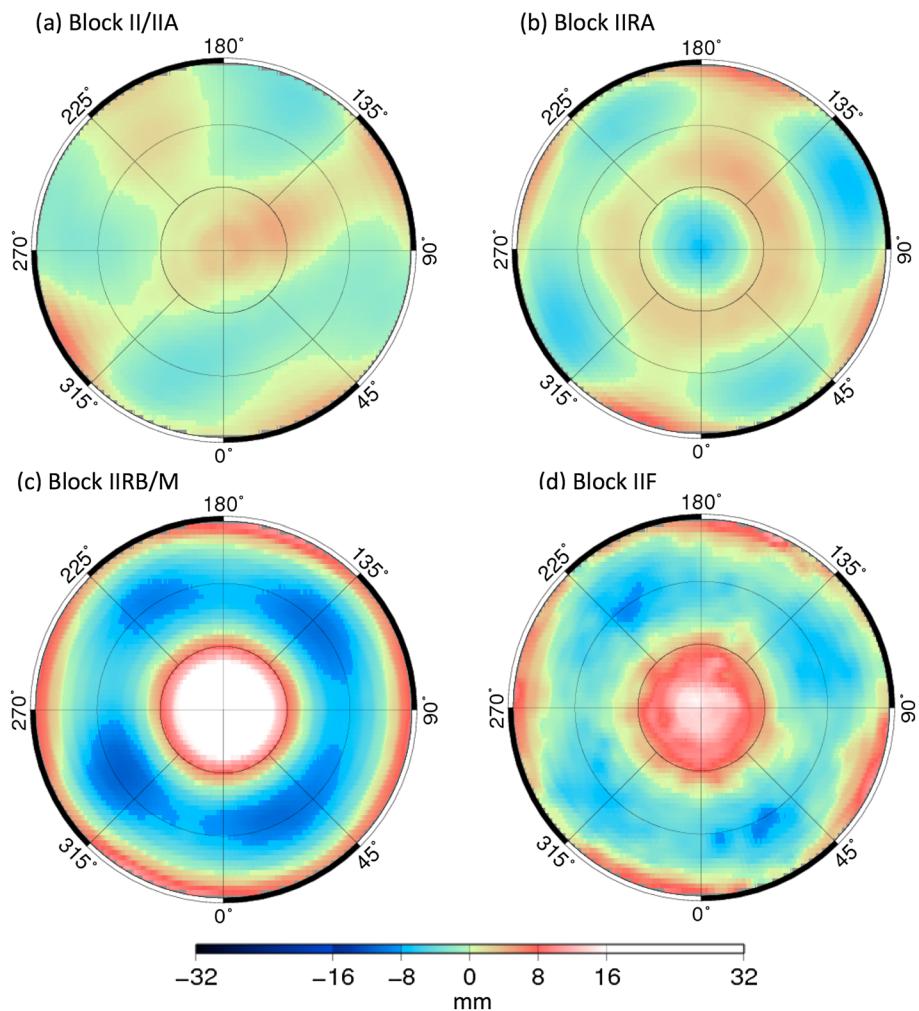


Figure 5. (a–d) GRACE-based GPS transmitter antenna phase variations (APV) as a function of nadir (0° – 15°) and azimuth (0° – 360°) angles for the four current antenna types. In all cases, the APV is for the ionosphere-free carrier phase (LC) and corresponds to the incremental delay with respect to a best fit antenna phase center (APC) from equiareal weighting. Based on GRACE LEO data, the estimates show important elevation-dependent differences. Azimuthal antenna variations depict the helical antenna elements [cf. Haines et al., 2004; Schmid et al., 2005], which are arranged in two concentric circles (cf. Figure 1).

and the inferred APC offsets are 1629 and 1693 mm for the GRACE- and robot-based estimates, respectively. The underlying techniques are quite different, with disparate limiting error sources. The robot calibration, for example, measured the antenna panel in isolation (cf. Figure 1) and thus could not capture any s/c multipath from the bulkhead, solar panels, and other appendages. A large fraction (90%) of the power, however, radiates from the central four helical elements (cf. Figure 1), for which the near field is comprised solely of other components of the antenna panel. The outer circle of helical elements transmits a weaker signal over a narrower beam [Aparicio et al., 1996]. It is thus conceivable that the fingerprints of phase multipath from the spacecraft bus (and panels) are faint in relation to the total APV_{CM} patterns as expressed in Figure 4. We note, however, that the azimuthal variations (GRACE versus robot) do not agree well, showing systematic dispersions at the 7 mm (RMS) level, linked to the positions of the antenna elements. This casts some doubt on the significance of the excellent agreement for the nadir-angle dependence, and the overall results of this particular comparison clearly warrant further investigation.

Provided in Figure 5 are the APVs for each of the four GPS satellite antenna types as a function of azimuth and nadir angle. For this depiction, the APV patterns are expressed as departures from the antenna phase center—rather than the spacecraft center of mass—in order to better expose systematic differences among

the satellite blocks. Larger departures from the phase center are observed for the modernized antenna panels on the IIR-B/M and F blocks. All four patterns reflect the helical antenna arrangement which is common to the GPS transmitters (cf. Figure 1).

2.4. Antenna Group Delay Variations From GRACE

Because our TRF solutions also employ ionosphere-free GPS pseudorange (PC) observations, we have developed estimates of the transmit antenna group-delay variations (AGV) to complement the APV calibrations. Due to the long effective wavelength (~ 30 m chip length), the code observations (PC) have higher intrinsic measurement noise and multipath than their phase counterparts (LC with ~ 10 cm wavelength). In recognition of this, we downweight the pseudorange significantly (e.g., 100x relative to phase) in most geodetic applications. Despite this, the range content of the code observations is useful and provides in particular the means to level estimates for both the phase biases and clock offsets. In contrast to phase multipath, code multipath can become more damaging as antenna height increases [Even-Tzur and Shaked, 2008], implying that GRACE likely provides a more favorable geometry than T/P for purposes of AGV calibration.

We generated the AGV calibrations by simple gridding of GRACE-B postfit (PC) POD residuals according to the azimuth and elevation of the transmitters. Data from two periods (October 2006 to November 2009 and October 2010 to June 2012) were used to ensure sufficient coverage of the GPS satellite blocks, including the new IIF satellites. The calibration estimates were iterated to convergence. While GRACE presents a favorable configuration for reducing code (PC) multipath, some corruption of the transmitter AGV calibrations is unavoidable. We expect this multipath contamination to manifest similarly across all recovered transmitter AGV patterns.

Figure 6 shows the GRACE-based AGV estimates for each of the GPS satellites participating in the TRF realizations. Noteworthy is the much larger amplitude of the AGV_{CM} (versus APV_{CM} , cf. Figure 4), especially for the Block IIR satellites. This block also shows large satellite-to-satellite variations, the general characteristics of which have been identified previously using both terrestrial and orbiter data [Springer and Dilssner, 2009; Haines et al., 2010]. These patterns, which are thought to originate from imperfect termination networks used in balancing the inner and outer arrays of helical antenna elements (cf. Figure 1), have also been observed for the Block IIR-M satellites using dedicated collections from a 3 m high-gain antenna in California [Tetewsky et al., 2014]. Due to the significant disparities among the AGV_{CM} patterns, we use satellite-specific calibrations for all Block IIR satellites. For other satellite antenna types (II/IIA and IIF), we use block averages.

3. Terrestrial Reference Frame Realization

To realize the TRF, we have developed an approach that capitalizes not only on the LEO-based APV and AGV estimates but also on a long-arc estimation strategy that attempts to tailor the GPS network solution for improved recovery of scale and origin. Detailed in Tables 3 and 4, this strategy features a GPS satellite precise orbit determination (POD) approach that is more dynamical than that used in routine production at JPL (<http://igscb.jpl.nasa.gov/igscb/center/analysis/jpl.acn>), which also supports the IGS combination process. The solution arcs are 9 days in length and centered on calendar weeks, implying 2 day overlaps between consecutive solutions. To better preserve the gravitational constraint on scale, updates to the satellite empirical accelerations (in solar coordinates) are made infrequently and only at the orbital resonant frequency of one cycle per revolution (1 cpr). Like the JPL production strategy, the orbit estimation problem is linearized about an accurate reference trajectory, and only a single iteration on the grand network solution is performed. In our case, the accurate reference solution is provided by 9 day dynamical fits to archival JPL products. To ensure there is no link to the TRF underlying the archival products, all parameters of the extended state vector used in creating this reference trajectory are re-estimated with no constraint in the grand solution (cf. Table 4).

To promote homogeneity in the ground component of the network, we used only stations equipped with antennas following the original JPL choke ring design, including the central Dorne Margolin element. (For a complete list of eligible antenna types, see <ftp://sideshow.jpl.nasa.gov/pub/urs/bjh/antennas.txt>.) For each weekly solution, we select from this eligible network up to 46 well-distributed stations by balancing two criteria: (1) minimize the isolation (great circle distance) of an arbitrary location on the globe from the nearest tracking site using the algorithm of Zumberge et al. [1994] and (2) minimize any asymmetry between the number of stations in the Northern and Southern Hemispheres. While a few short outages are acceptable, the surviving stations must track nearly continuously for the 9 days represented in each solution arc. Following

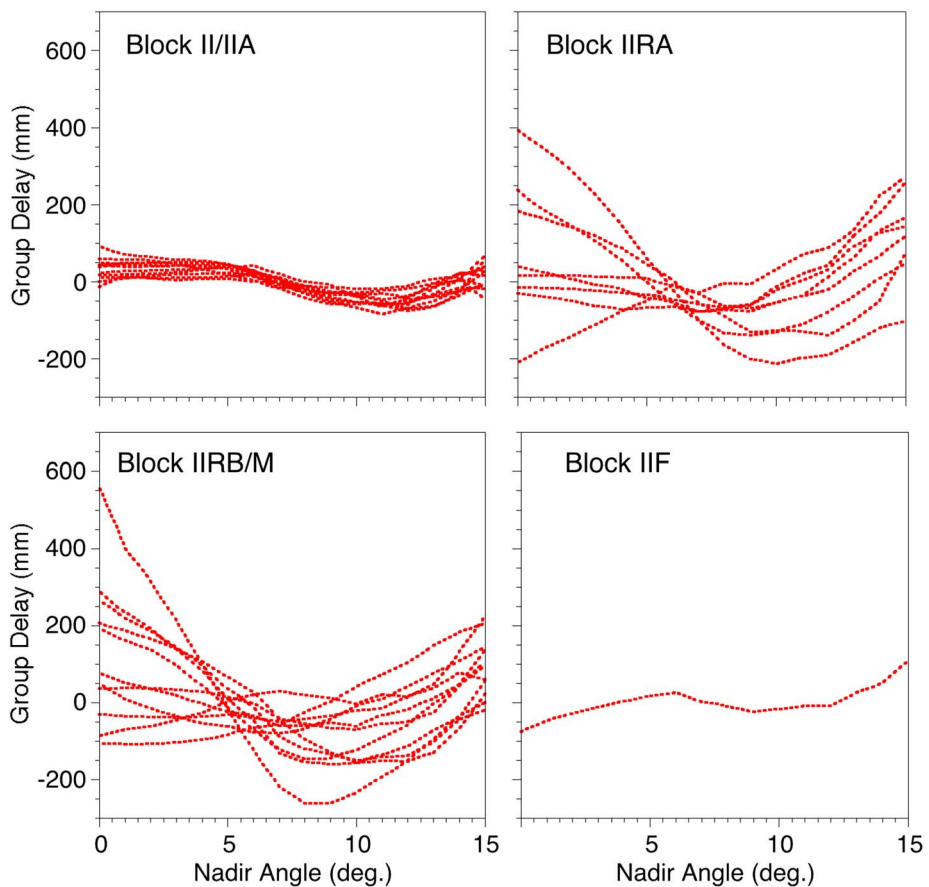


Figure 6. GPS transmitter antenna group delay variations (AGV_{CM}) as a function of nadir angle for current GPS satellites. In all cases, the group delay is for the ionosphere-free carrier pseudorange (PC) and corresponds to the total delay with respect to the spacecraft center of mass (CM). The Block IIR satellites show important satellite-to-satellite variations.

these criteria, a typical isolation of 2000 km or less is achieved in the 2000–2014 time frame, with equal numbers of stations in the Northern and Southern Hemispheres. Prior to 2000, the isolation increases gradually for progressively older tracking data sets. Our solutions span the 1997–2013 time frame, but no earlier, in order to avoid difficulties linked to the distribution and quality of ground data from the early GPS network. Typical network distributions for 1997 (30 stations) and 2013 (46 stations) are provided in Figure 7 and depict the improved tracking coverage over 16 years.

The phase properties of the prototypical (TurboRogue) JPL choke ring ground antenna were measured at the JPL test range in 1993 under nearly the same conditions as the T/P antenna [Young *et al.*, 1993]. To ensure consistency, we use in our nominal approach the elevation-averaged TurboRogue APV from this experiment. To describe the nadir angle dependence of the GPS APVs, we take the average of the T/P- and GRACE-based results (Figure 4). The azimuthal variations, being well determined in the estimation process, are taken solely from GRACE (Figure 5). Recognizing the large sensitivity (few ppb) of the absolute TRF scale to choices for the APV models [Haines *et al.*, 2010, 2011], we also discuss departures from this nominal approach (cf. section 4).

The overall estimation strategy features minimal a priori constraints on all station coordinates, satellite epoch states, and Earth Rotation Parameters (ERP). As the ERPs are fundamentally linked to both the definition and utility of the TRF, the attendant estimation strategy warrants some additional discussion. The position of the pole (x_p, y_p) and Universal Time (UT1 – UTC) are estimated as loosely constrained random walk processes, with updates every 2 h. As absolute UT1 is poorly observed by satellite techniques due to correlation with the orbital nodes [e.g., Gambis and Luzum, 2011], the initial value of UT1 – UTC is tightly constrained to the a priori (Bulletin A) value, and the GPS data dictate the variation of UT1 over the course of each 9 day solution. Because all station coordinates are estimated in our network strategy, the mean pole position is also poorly observed. As with UT1, however, the variations of the pole position embodied by the random walk updates are

Table 3. GPS-Based Network Strategy for TRF Realization: Background Models

	Source/Value	Reference
<i>GPS Satellite Models</i>		
Spacecraft attitude	GYM95	Bar-Sever [1996]
Static geopotential field	GGM02C (12 X 12)	Tapley <i>et al.</i> [2005]
Ocean tide potential	FES2004	Lyard <i>et al.</i> [2006]
Solid tide potential	IERS2010	Petit and Luzum [2010]
Third-body potential	DE405	Standish [1998]
Solar radiation pressure	GSPM13	Sibois <i>et al.</i> [2014]
Earth radiation pressure	UT Albedo + IR	Knoche [1989]
Antenna thrust	IGS ^a	
Transmitter APV	LEO-based	This study
Transmitter AGV	LEO-based	This study
<i>Ground Station Models</i>		
Earth tide	IERS2010	Petit and Luzum [2010]
Pole tide	IERS2010	Petit and Luzum [2010]
Ocean loading (except Ssa)	FES2004	Lyard <i>et al.</i> [2006]
Ocean loading (Ssa ^b)	Equilibrium	Petit and Luzum [2010]
Zenith dry troposphere	GPT ^c	Boehm <i>et al.</i> [2007]
Zenith wet troposphere	10 cm	(a priori only)
Troposphere mapping functions	VMF1	Boehm <i>et al.</i> [2006]
Ionosphere	Second order	Garcia-Fernandez <i>et al.</i> [2013]
Receiver APV	JPL test range	Young <i>et al.</i> [1993]
<i>Global Parameters</i>		
Earth orientation	Bulletin A	Petit and Luzum [2010]
High-frequency earth orientation	IERS2010	Petit and Luzum [2010]
Precision/nutation	IAU 2006	Petit and Luzum [2010]

^a<http://acc.igs.org/orbits/thrust-power.txt>.^bSolar semiannual.^cGlobal pressure and temperature model.

well determined by the GPS data. The frequent (2 h) updates to the ERP parameters are intended to provide a framework for better characterizing the response of the Earth system to various high-frequency geophysical signals, such as tides and earthquakes [Sibois, 2011].

This fiducial-free solution strategy ensures the scale and origin of the ground network are fully inherited from the GPS data themselves, with underpinning from the GPS radio propagation models and dynamical constraints on the GPS satellite motions [Heflin *et al.*, 1992]. Our solutions thus provide the means to realize both the origin and scale of the TRF on a quasi-instantaneous (i.e., weekly) basis, independent in practice of SLR and VLBI. While the standard Earth geocentric gravitational constant (GM) used in this study is derived from SLR [Ries *et al.*, 1992], this constant is considered fundamental. The background solar radiation pressure (SRP) model also has a subordinate dependence on SLR and VLBI, but a competitive TRF can be realized with no background GPS SRP model whatsoever. A more complete treatment of this result, and of the independence of the background force models in general, is provided in the Appendix.

The constraint of UT1 – UTC to Bulletin A (and thus VLBI) at the initial epoch provides an accurate starting point for the random walk departures of UT1 – UTC driven by the GPS updates and has negligible impact on realizing the fundamental TRF parameters. VLBI remains essential for accurate measurements of UT1 and provides the only accurate means of relating the TRF to the celestial reference frame [e.g., Gambis and Luzum, 2011].

To evaluate the quality of our solutions, we compare each weekly GPS frame to ITRF2008 by estimating the seven parameters of a similarity (Helmert) transformation using common stations [e.g., Blewitt *et al.*, 1992].

Table 4. GPS-Based Network Strategy for TRF Realization: Estimation Strategy

Estimated Parameter	Parameterization	σ	σ_p
GPS epoch states			
Position (x_0, y_0, z_0)		10^{30} km	—
Velocity ($\dot{x}_0, \dot{y}_0, \dot{z}_0$)		10^{30} km s $^{-1}$	—
GPS radiation pressure coefficient (C_R)	Bias	100	—
GPS Y bias	Bias	100 nm s $^{-2}$	—
GPS empirical 1/rev accelerations ^a			
Sun direction	36 h updates with $\tau = 7$ days	1 nm s $^{-2}$	0.1 nm s $^{-2}$
EPS Y direction	36 h updates with $\tau = 7$ days	1 nm s $^{-2}$	0.1 nm s $^{-2}$
GPS empirical down-track acceleration	1 day updates; random walk	1 nm s $^{-2}$	3 pm s $^{-2}$ s $^{-1/2}$
GPS yaw rates	Bias per midnight turn	0.01° s $^{-1}$	—
Ground station coordinates	Bias	1 km	—
Ground zenith wet troposphere	5 min updates; random walk	0.5 m	3 mm h $^{-1/2}$
Ground wet troposphere gradient	5 min updates; random walk	0.5 m	0.3 mm h $^{-1/2}$
UT1 – UTC	2 h updates; random walk	1 ms	1.2 μ s h $^{-1/2}$
X/Y pole	2 h updates; random walk	1 rad	$0.1''$ h $^{-1/2}$
Clock offsets	5 min updates; white noise	1 s	1 s
Carrier-phase biases	White-noise update at breaks	3×10^5 km	3×10^5 km
Tracking Data		σ	Rate
Ionosphere-free carrier phase: LC = $2.54(L1) - 1.54(L2)$		1 cm	5 min
Ionosphere-free pseudorange: PC = $2.54(P1) - 1.54(P2)$		100 cm	5 min

^aIn Earth-Probe-Sun (EPS) coordinates, with shadow factor (i.e., off in eclipse).

(Strictly speaking, we use the current IGS realization of ITRF2008. Referred to as IGB08, this frame is derived by selecting a subset of stable and well-determined GNSS stations from ITRF2008 [e.g., Rebischung *et al.*, 2012]. Small position corrections are made to account for ground antenna calibrations, but the origin and scale remain aligned to the values inherited from SLR and VLBI via ITRF2008.) Represented in the 17 year time series of weekly transformation parameters is a convolution of errors from both the ITRF and the quasi-instantaneous GPS frame.

Benefits of a long-arc strategy are illustrated in Figure 8, which provides color perspectives of the correlation matrices for the three origin (geocenter) parameters using 30 h and 9 day solutions. In order to produce the estimates underlying this notional diagram, we fixed station coordinates to ITRF2008 and explicitly estimated the 3-D geocenter (origin) offset. This alternative approach to realizing the origin of the GPS network implies that the geocenter estimates and their uncertainties are accessible in the normal equations formed as part of the estimation process, enabling direct examination of the correlations with other estimated parameters. After 30 h—the arc length adopted for the standard JPL submission to the IGS [Desai *et al.*, 2011]—correlations of the geocenter estimate with clock and orbital parameters stand out. These “hot spots” in the correlation matrix are symptomatic of known weaknesses in the GPS measurement system related to the differential nature of the observations and difficulties in modeling the orbital dynamics [e.g., Kuang *et al.*, 1996; Meindl *et al.*, 2013; Rebischung *et al.*, 2013; Kuang *et al.*, 2015]. After 9 days, the correlations are significantly reduced, particularly those linked to the GPS orbit states and associated empirical accelerations. The 9 day solution has the advantage that it spans 18 full revolutions of the GPS satellites about the Earth (versus 2.5 revolutions for the 30 h solution), implying improved observability of orbit errors at the satellite resonance frequency of 1 cpr. Also important, the elevation angle of the Sun relative to the GPS orbital plane (β_s) can vary significantly (by close to 9°) over the course of a 9 day solution, which helps to decorrelate solar radiation pressure errors from the geocenter [Meindl *et al.*, 2013]. We note that correlations between the geocenter and the GPS satellite clock offsets remain discernible in the 9 day solution. Tighter constraints on the satellite clocks—presently estimated every measurement epoch using white noise updates—may alleviate this [Rebischung *et al.*, 2013]. Our initial attempts at constraining the GPS satellite clocks have not yielded satisfactory results, especially for the legacy satellites, but this remains a subject of ongoing research.

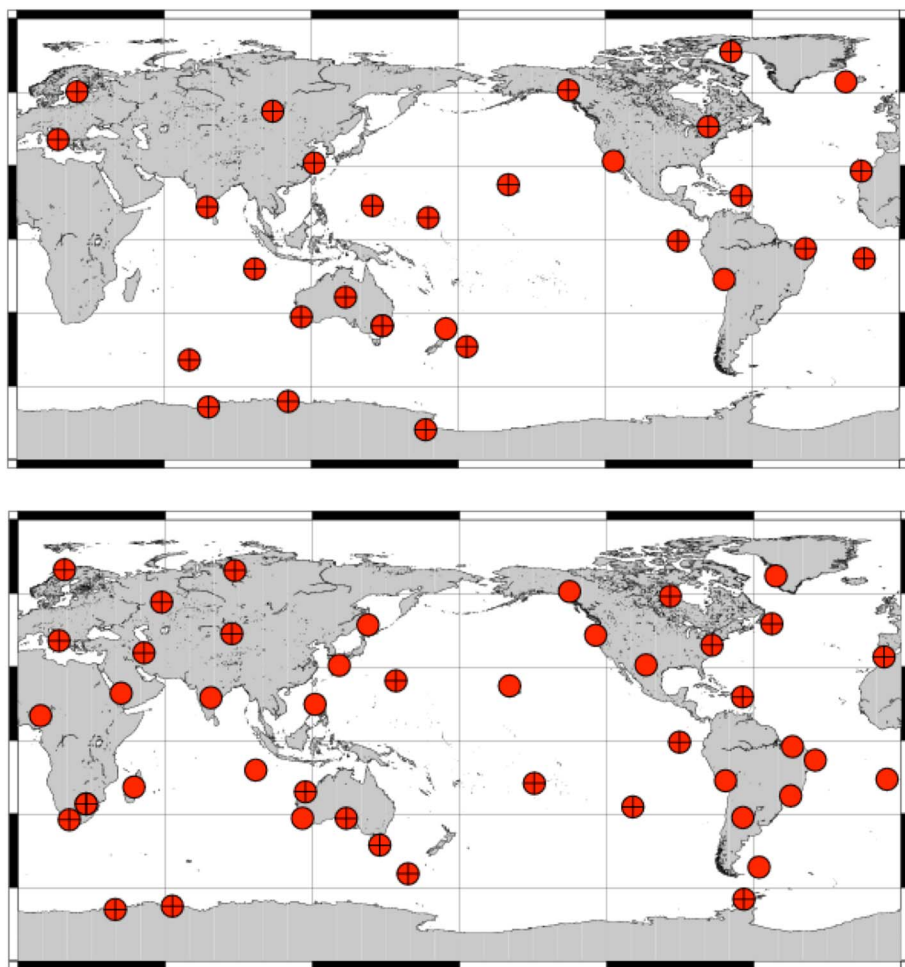


Figure 7. Ground network distribution for weekly solutions beginning 22 January 1997 and 23 October 2013. Stations denoted with plus signs are also represented in the independent IGS (IGb08) realization of the ITRF2008 [Altamimi *et al.*, 2011; Rebischung *et al.*, 2012] for the time period in question. Due to aging of the current ITRF, a significant fraction of the stations comprising the October 2013 network (21 of 46) are not candidates for the Helmert transformation used to compare the two TRF realizations. (Stations that experienced discontinuities—due to equipment changes and earthquakes—after the release of ITRF2008 are excluded.)

3.1. Results: Scale

In comparing our quasi-instantaneous GPS realizations of the frame with ITRF2008, we consider first the relative scale of the systems (Figure 9). The trend of $+0.03 \text{ ppb yr}^{-1}$ (GPS scale increasing with respect to ITRF2008) corresponds to only $+0.2 \text{ mm yr}^{-1}$ at the Earth's surface. This small relative drift is close to the estimated error of ITRF2008 [Altamimi *et al.*, 2011; Argus, 2012; Collilieux *et al.*, 2014], implying we cannot identify which of the underlying geodetic techniques (VLBI/SLR or GPS) is preferred for long-term scale stability. Though we can discern some small interannual variations in the time series, there is no evidence of the abrupt ($\sim 1 \text{ ppb}$) scale instabilities which originally implicated the GPS satellite antenna models as significant error sources [Ge *et al.*, 2005]. While some of the remaining systematic variations could be due to the changing composition of the GPS constellation and ground network, these discrepancies may also stem from the aging of ITRF2008. A small (1 mm) annual signal is evident and may be due to aliasing of crustal loading linked to the imperfect global sampling of the GPS stations. The repeatability of the weekly GPS solutions is at the 0.3 ppb level (2 mm), testifying to the potential strength of GPS for realizing scale when systematic errors can be carefully controlled.

Also noteworthy in Figure 9 is the relative scale bias of 1.1 ppb at epoch (2005.0), which amounts to 7 mm at the Earth's surface. We consider this level of agreement with the VLBI/SLR combined scale somewhat fortuitous, as the absolute GPS scale is highly sensitive to the particular pairing of APV calibrations for the GPS satellites and

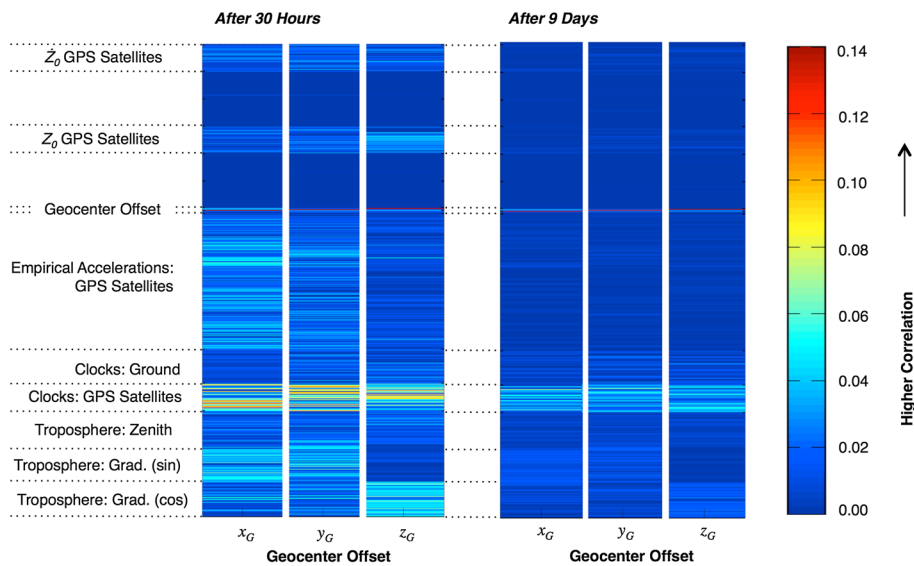


Figure 8. Correlation matrices for 3-D geocenter offset estimates from a representative GPS-based network solution (4 March 2011 epoch) using two arc lengths: (left) 30 h and (right) 9 days. Absolute values of the correlations, ranging from 0 to 1, are provided in rainbow colors, but the scale saturates at 0.14 to better highlight differences for the most common occurrences. Over 500 estimated parameters are represented along the vertical axis, and text labels (on the left) highlight particular parameter groupings responsible for the highest correlations with geocenter. \dot{Z}_0 and Z_0 refer respectively to the epoch position and velocity of the GPS satellite along the Earth's spin axis. The long arc helps to combat some of the correlations (e.g., with troposphere, clock, and orbital parameters) that plague GPS-based realizations of the frame [e.g., Kuang et al., 1996; Meindl et al., 2013; Rebischung et al., 2013]. The estimates of the geocenter offsets are in keeping with the expected noise of the determinations: (x_g, y_g, z_g) of $(0.5, 0.9, -1.5)$ and $(-4.2, -4.2, 1.4)$ in millimeters for the 30 h and 9 day solutions, respectively.

ground stations. In practical terms, errors in the absolute scale carry much less consequence for global change monitoring than errors in the scale rate. Discrepancies in the GPS scale bias, however, do warrant additional investigation as they provide important clues on the source of remaining antenna calibration errors, including multipath effects (cf. section 4).

3.2. Results: Origin and Geocenter Motion

We draw a distinction between locating the origin along the equatorial (X , Y) axes and along the spin (Z) axis, as the latter represents a greater challenge for satellite geodetic techniques [e.g., Kuang et al., 2015]. Figure 10 provides comparisons of the quasi-instantaneous (weekly) GPS origin with ITRF2008 along the X and Y equatorial axes, respectively. In terms of both offset and rate, the differences along both axes are within the expected errors of ITRF2008, for which the origin is realized solely by SLR.

By convention, the time evolution of the current ITRF is constrained to be linear. The origin is designed to coincide with the center of mass (CM) of the Earth system over the long term, but it actually resembles the Earth center of figure (CF) on seasonal (and shorter) timescales [Dong et al., 2003]. Our GPS solutions, on the other hand, are designed to realize the quasi-instantaneous CM for the week in question, implying that departures of our solutions from the ITRF should contain the expression of periodic (e.g., annual) geocenter motion. The annual fluctuations of CF with respect to CM are small (few mm) and can be attributed to seasonal redistribution of water within the Earth's fluid envelope [e.g., Wu et al., 2012]. Lavallée et al. [2006] describe some limitations associated with the direct recovery of annual geocenter motion from GPS and caution that the “network shift” approach embodied in the Helmert transformation performs particularly poorly [cf. Dong et al., 2003]. Some investigators [e.g., Rebischung et al., 2013] harbor serious doubts concerning the ability of GPS to directly sense the small translations at all, citing damaging correlations linked to fundamental weaknesses in the GPS tracking measurements.

To provide perspective on the accuracy of our annual geocenter motion results, we overlay in Figure 10 estimates from an independent source. Wu et al. [2013] determined monthly geocenter displacements from an inverse technique, which processed GRACE gravity data, models of ocean bottom pressure, and load deformations from degrees 1 to 60 (spherical harmonic coefficients for $n = 1$ to 60) from GPS stations. The deformation

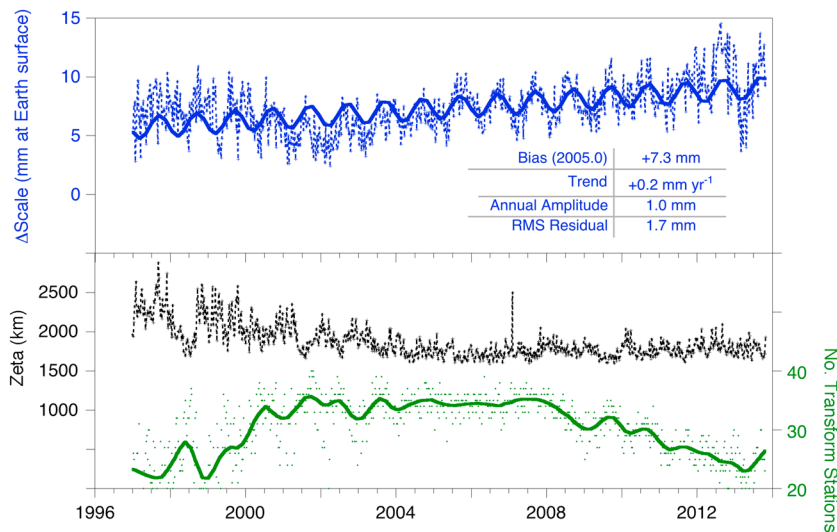


Figure 9. (top) Scale comparison for TRF: quasi-instantaneous (weekly) GPS solutions (this study) minus long-term VLBI/SLR as manifest in the ITRF2008/IGb08 solution [e.g., Rebischung *et al.*, 2012]. A fit of the weekly differences to linear and annual signals is shown (solid blue line). (bottom) The RMS-distance-to-nearest-site function (ζ), which provides a measure of the isolation of an arbitrary location on the globe from the closest tracking site [Zumberge *et al.*, 1994], along with the number of eligible stations participating in the Helmert transformation underlying the frame comparison. While the GPS network distribution is stable after 2004, the number of stations used in the transformation decreases after 2008 due to aging of the ITRF. (In particular, an anomalous discontinuity occurring after the publication of the frame renders a station ineligible.) Some of these slow changes in network composition may provide an explanation for the systematic behavior in the scale comparison. The overall drift of 0.2 mm yr^{-1} is nonetheless commensurate with the estimated uncertainty in the current ITRF [Wu *et al.*, 2011; Collilieux *et al.*, 2014].

approach provides an indirect measure of geocenter motion from the GPS network. Only relative crustal displacement information contributes to the solution; any geocenter translation vanishes from the network solutions in aligning to the ITRF. The geocenter motion is then inferred from these relative crustal displacements through knowledge of the load Love numbers [Blewitt *et al.*, 2001; Dong *et al.*, 2003; Wu *et al.*, 2012]. The estimates from the inverse model of Wu *et al.* [2013] are considered representative of competing models that typify the current state of the art [c.f. Table 2 of Wu *et al.*, 2012].

Along the Y axis, the correlation between the two estimates (GPS versus inverse) is unmistakable: the amplitude agrees to better than 1 mm (3.6 and 2.9 mm respectively for the GPS and inverse solutions), while the phase agrees to 2 days (with the seasonal signal peaking 24 November and 22 November, respectively). Along the X axis, the agreement is less compelling: the amplitude agrees to 1.2 mm (0.8 and 2.0 mm), but the phase is shifted (13 October and 18 February). The annual geocenter motion along the X axis has a particularly small amplitude (<1 mm) for the GPS solution, implying a higher uncertainty on the phase. If we express the annual geocenter motion as a vector in the equatorial plane, however, we find excellent overall agreement: the GPS annual signal has a peak amplitude of 3.7 mm toward 99°E on 23 November, while the inverse method yields a peak amplitude of 3.0 mm toward 92°E on 16 November. The peak variation in both cases is close to the $\pm Y$ axis, which lies near regions of particularly high seasonal groundwater variability such as the Amazon basin and central Asia.

Turning to the Z (spin-axis) component of the origin, we show in Figure 11 (top) that the time series of GPS solutions agrees well with ITRF2008 in terms of both offset (4 mm) and rate ($+0.3 \text{ mm yr}^{-1}$). As with the equatorial (X, Y) components, these long-term differences are in keeping with the uncertainty of ITRF2008 [Wu *et al.*, 2011; Argus, 2012; Collilieux *et al.*, 2014], implying it is not possible on this basis to identify which solution is preferred.

In contrast to the comparisons for the equatorial plane, however, the differences along the Z axis show significant periodic variations at the GPS β_s period (~ 351 days) and odd overtones thereof (Figure 12, top). Spurious GPS signals at these periods—now commonly called “draconitic” errors—are due in part to residual orbit

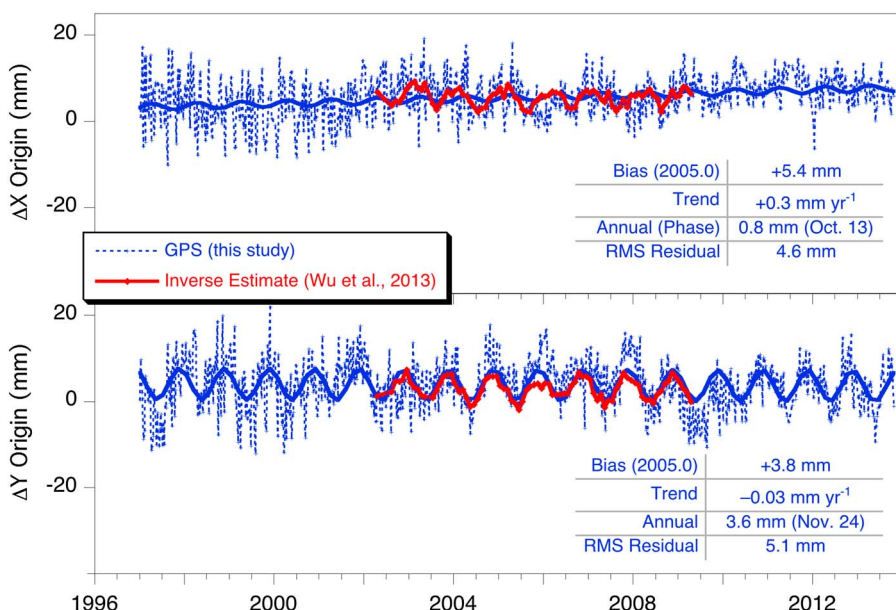


Figure 10. Comparison of TRF origin along (top) X and (bottom) Y equatorial axes: quasi-instantaneous (weekly) GPS origin (this study) minus long-term SLR origin as manifest in the ITRF2008/IGb08 solution [e.g., Rebischung et al., 2012]. A fit of the weekly differences to linear and annual signals is shown (solid blue line). The total (2-D) equatorial offset and drift of 7 mm and 0.3 mm yr^{-1} , respectively, are commensurate with the estimated uncertainty in the ITRF. At annual frequencies, the departures of the quasi-instantaneous (weekly) GPS solutions should contain the expression of geocenter displacement due to seasonal redistribution of water mass within the Earth's fluid envelope [Wu et al., 2012]. The red overlay line provides independently derived estimate of geocenter motion (CM – CF) from an inverse method [Wu et al., 2013]. Taken together, the direct GPS determinations for the X and Y axes yield a peak amplitude of 3.7 mm toward 99°E on November 23. Results for the inverse approach are in good agreement, yielding a peak amplitude of 3.0 mm toward 92°E on November 16.

errors from mismodeled solar radiation pressure [Meindl et al., 2013; Rodriguez-Solano et al., 2014]. The manner in which measurement model errors (e.g., antenna multipath) manifest as β_s varies [Ray et al., 2008] may also contribute.

The spin (Z) axis is particularly vulnerable to these effects: along the equatorial (X , Y) axes fixed to the Earth, systematic GPS errors locked in phase with the position of the Sun will average down over a period of days as the Earth rotates within the Earth Probe-Sun (EPS) frame [e.g., Kuang et al., 2015]. No such averaging benefit is incurred along the Z axis, and the quasi-instantaneous frame is subjected to spurious periodic translations at draconitic periods. Because the β_s period is close to one solar year, the large ($\sim 8 \text{ mm}$) draconitic signal in our solution modulates the annual signal and obscures the fingerprints of periodic geocenter motions along the Z axis (Figure 11, top). While the series is sufficiently long to estimate simultaneously annual and draconitic variations, the recovered amplitude and phase of the former remain quite sensitive to the assumed period of the latter. Adopting 351 days for the β_s period yields an estimate of 4.6 mm for the amplitude of the annual (geocenter) signal, which is very close to the comparable figure (4.3 mm) from the inverse solution [Wu et al., 2012]. The annual phase, however, is shifted by more than a season, with the GPS signal peaking 4 months earlier (on 9 October). A close examination of the periodogram (Figure 12, top) actually reveals a curious lull in the energy at the annual period, surrounded by peaks close to 350 and 380 days, reinforcing that our results for the annual (Z) geocenter motion are not robust.

3.3. Impact of LEO Measurements

One way to improve the sensitivity of GPS to geocenter motion along the Z axis is to supplement data from the terrestrial network with observations from GPS receivers carried in low Earth orbit [cf. Malla et al., 1993b]. The rapidly moving baselines formed between the ground stations and orbiting receiver markedly improve the spatial and temporal diversity of the network, subverting systematic errors linked to the repeating geometries of the rotating Earth, Sun, and GPS orbital planes. As quantified in simulations by Kuang et al. [2015], correlations between geocenter and other parameters are significantly diminished. Processing 4.5 years of GRACE GPS data in daily solutions, Kang et al. [2009] determined annual geocenter variations that compared

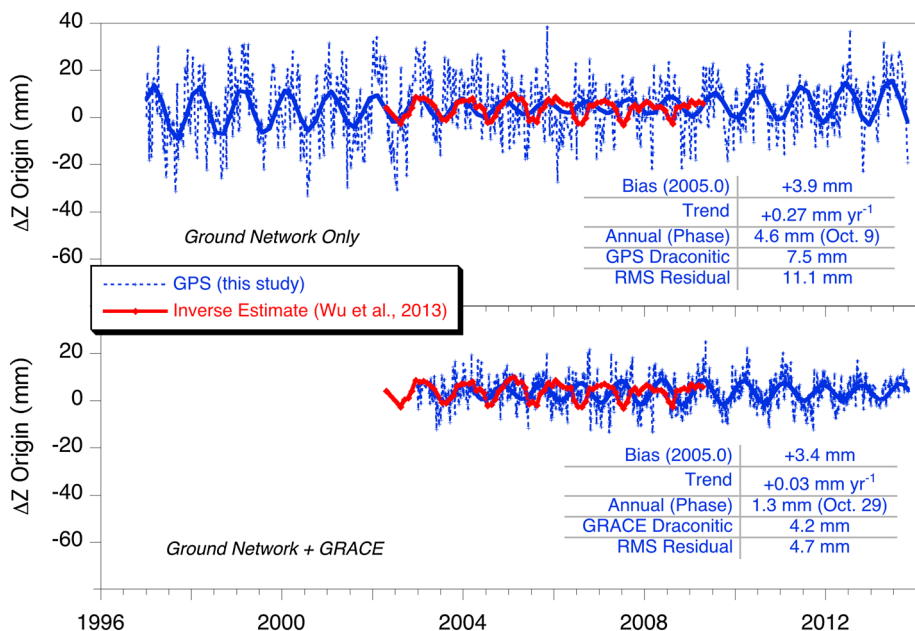


Figure 11. Comparison of TRF origin along the Earth Z (spin) axis: quasi-instantaneous GPS origin (this study) minus long-term SLR origin as manifest in the ITRF2008/IGb08 solution [e.g., Rebischung *et al.*, 2012]. The top panel depicts the results from our nominal approach, which uses data from up to 46 stations in 9 day solution arcs. The bottom panel shows the result when LEO data from GRACE are used to supplement the ground network in 3 day solution arcs. Both approaches provide frame realizations that are competitive with the ITRF in terms of origin offset and long-term stability. Determining annual geocenter motion along the Z axis is challenging due to the prevalence of spurious signals at the GPS draconitic period of ~ 351 days [e.g., Rodriguez-Solano *et al.*, 2014]. Adding GRACE to the network dramatically improves the repeatability of the weekly TRF realizations but introduces some signal at the GRACE draconitic (β_3) period. The solid blue lines show (top) least squares fits to annual + GPS draconitic and (bottom) annual + GRACE draconitic. The red overlay line provides independently derived estimates of geocenter motion (CM – CF) from an inverse method [Wu *et al.*, 2013].

favorably with independent measures, except in the phase of the Z geocenter. Our results—first described in abstracts [e.g., Haines *et al.*, 2011; Weiss *et al.*, 2013]—are based on incorporation of the GPS LEO data directly in our long-arc network solutions. We estimate the orbits of all participating satellites, including the LEO, together with the coordinates of the stations comprising the ground network.

To illustrate the potential impact of LEO data on the Z geocenter, we supplement the ground network used in our nominal solution with GPS flight data from the near-polar (89.5° inclination) GRACE-A satellite for 2003–2013. Due to current software limitations, the solutions incorporating GRACE are limited to 3 days in length, but the overall strategy otherwise follows Table 3. For GRACE itself, the POD strategy closely follows Table 1, which describes a quasidynamical approach designed to support antenna calibrations (cf. section 2.3). Noteworthy differences are the weighting of the data and the use of both ionosphere-free phase (LC) and pseudorange (PC) data for GRACE. In order to increase the influence of the GRACE data against the backdrop of 46 ground stations, we decreased the (1σ) data uncertainty for GRACE LC measurements from 10 to 2 mm, while maintaining the comparable figure for ground stations at the 10 mm level. We treated the PC data similarly, setting σ at 20 and 100 cm for GRACE and ground data, respectively.

As shown in Figure 11, the addition of GRACE dramatically improves the repeatability of the quasi-instantaneous realizations of the Z origin: the postfit RMS residual is reduced from 11 to 5 mm, which represents an 80% reduction in variance, and implies the repeatability is comparable to that observed for the X and Y axes (cf. Figure 10). Controlled tests using the same (3 day) arc length with and without GRACE support that the improvement is due almost entirely to the addition of GRACE [e.g., Weiss *et al.*, 2013]. While the time series including GRACE is shorter, it also shows excellent stability relative to ITRF2008 (<0.1 mm difference in rate between 2003 and 2013).

While the improved repeatability can be attributed to lower errors across most of the frequency spectrum (Figure 12), particular improvement is noted at the GPS draconitic period bands. When GRACE data are added,

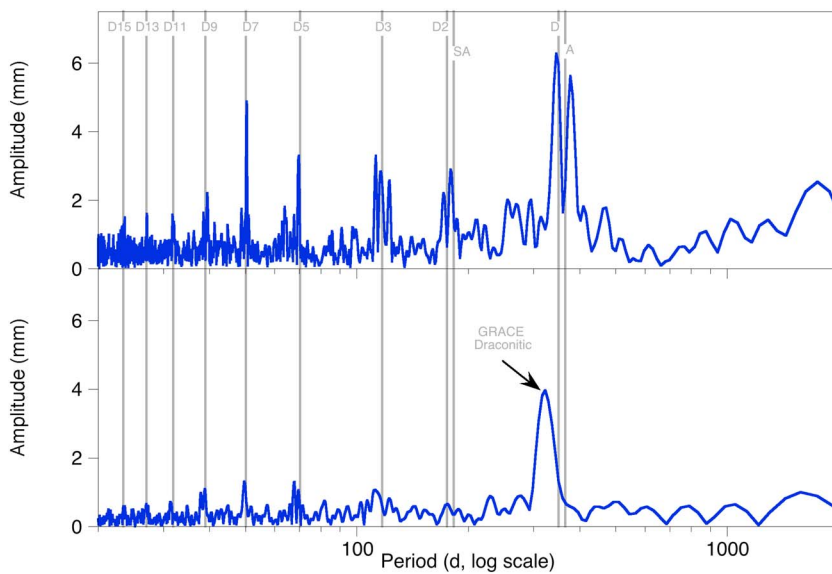


Figure 12. Lomb-Scargle periodograms for estimated geocenter motions along Earth Z (spin) axis, as depicted in Figure 11. Estimates from ground network data alone show spurious variabilities at the GPS draconitic period and odd overtones thereof (D_N , where $N = 1, 15$). Supplementing the ground network with the GRACE low Earth orbiter significantly improves the repeatability of the solutions and practically eliminates GPS draconitic variations. However, new (weaker) signals linked to the GRACE orbit β_s variations emerge.

spurious signals linked to the GPS β_s period practically vanish. At the same time, weaker signals emerge at the GRACE β_s period (~ 320 days) and overtones thereof. Somewhat unexpectedly, we find little energy at the annual period where we anticipate evidence of seasonal water mass redistribution between the Northern and Southern Hemispheres. The amplitude of the annual geocenter signal (Z) is 1.3 mm, much smaller than expected from the inverse solution (4.3 mm). In describing the reprocessed JPL submission to IGS, Desai *et al.* [2014] also report unexpectedly small (<2 mm) annual geocenter variations along the spin axis and speculate the attenuation of this signal may have been aggravated by the update to the background solar radiation pressure (SRP) model for the GPS satellites [GSPM13, Sibois *et al.*, 2014]. These background SRP models are empirical, and their capacity to absorb periodic geophysical signals—especially annual variations along the Z axis—warrants further investigation (cf. Appendix).

While the main impact of GRACE is observed along the Z axis, the data are also also expected to prove favorable for other fundamental parameters of the TRF. Provided in Table 5 are statistics on the comparisons of the two GPS-based TRF solutions (nominal and GRACE enhanced) to the IGb08 realization of ITRF2008. The lower postfit residuals indicate that the quasi-instantaneous TRF realizations using GRACE have better short-term stability. Given the current uncertainty in the ITRF, however, the long-term fit parameters are presently too close to distinguish a preferred approach. The results nonetheless reinforce that GPS data alone, whether enhanced with GRACE data or not, can be used to realize a state-of-the-art TRF. Estimates of the annual geocenter motion along the equatorial plane are also robust, having shifted only slightly under the influence of the GRACE GPS data in the updated solution strategy.

Table 5. Comparison of GPS-Based TRF With ITRF2008/IGb08: Nominal Versus GRACE^a

Fit Parameter	Scale	X	Y	Z
Δ Bias (2005.0, mm)	7.3/6.9	5.4/3.5	3.8/3.0	3.9/3.4
Δ Rate (mm yr^{-1})	0.2/0.3	0.3/0.2	-0.0/-0.0	0.3/0.0
Annual amplitude (mm)	1.0/1.0	0.8/0.6	3.6/3.4	4.6/1.3
Annual phase (day of year)	77/54	286/301	328/337	282/302
Postfit residual (mm)	1.6/1.2	4.6/3.3	5.1/3.5	11.1/4.7

^aEach pair of numbers in table represents nominal/GRACE result, where the nominal time series spans 1997–2013 and the GRACE-enhanced time series spans 2003–2013.

4. Summary and Future Work

We have developed a TRF using GPS ground network data collected from 1997 to 2013 and have taken careful measures to ensure independence of the origin and scale from both SLR and VLBI. This has provided new insights on limiting GPS error sources, such as mismodeled antenna calibrations, and is expected to help inform decisions on the contribution of GPS in multitechnique frame realizations. At the foundation of our solution are calibrations of the GPS transmitter antenna phase and group delay variations derived from GPS observations taken in low Earth orbit by the GRACE and TOPEX/Poseidon (T/P) missions. Precise orbit determination (POD) techniques are used to estimate the average distance between the centers of mass of the Earth and satellites (both GPS and LEO) with accuracies at the centimeter level, and with negligible sensitivity to the scale and origin of any extant TRF. Together with a priori models for the GRACE and T/P GPS antennas, this information provides the means to accurately calibrate the phase and group delay variations of the GPS satellite antennas.

In addition to the antenna calibrations, we have developed a long-arc network solution strategy that is tailored to reference frame realization and designed to better overcome some of the inherent weaknesses of the GPS observations. Time series of quasi-instantaneous (weekly) TRF realizations based on this long-arc strategy testify to the quality of the GPS observations when processed in the manner. In terms of long-term (secular) stability, the GPS-based TRF is indistinguishable from ITRF2008 at the published error levels. In particular, the scale rate agrees to 0.03 ppb yr^{-1} (0.2 mm yr^{-1} at the Earth's surface) and the origin rate (3-D) to 0.4 mm yr^{-1} . The two frames (GPS and ITRF2008) are also competitive in absolute terms: the GPS scale is larger (higher) than the ITRF2008 scale by 1.1 ppb (7 mm at the Earth's surface), and the 3-D origin is translated by only 8 mm, though the agreement of the former (discussed below) is somewhat serendipitous.

Quasi-instantaneous (weekly) GPS realizations of the Earth CM afford the opportunity to monitor small (few-mm) annual geocenter motions associated with redistribution of water within the Earth's fluid envelope. Along the equatorial plane, the GPS estimates agree well with state-of-the-art estimates. Along the spin (Z) axis, the estimate of annual geocenter motion is not robust, due in part to significant errors linked to the β_s (draconitic) period of the GPS satellites. By adding GRACE to the network, we virtually eliminated these errors and reduced the variance of the quasi-instantaneous (weekly) estimates of Z geocenter by 80%. However, the improvement came at some cost, as error signals were introduced at the GRACE β_s period, which may also obscure real annual variations.

In terms of future work, additional studies on the APV models are warranted for both the GPS satellites and the ground receivers. As noted previously (cf. section 3.1), the apparent accuracy of the absolute scale realized by our GPS solutions is somewhat fortuitous. The scale bias is highly sensitive to the systematic elevation dependencies established by the pairing of APV models for the transmitters and receivers. While the elevation-dependent GRACE- and T/P-based APV patterns (Figure 4) agree to 7 mm (LC, 1σ), these modest differences explain a scale offset of 5 ppb as realized by the global ground network. Similarly, competing estimates for the APV of the ground choke ring antenna (robot versus JPL outdoor test range) agree at the 5 mm level (LC) in terms of elevation dependence but explain a scale bias of 4 ppb. Fortunately, these same APV choices have a much smaller influence on the scale stability: in controlled tests, T/P-based calibrations yielded a scale rate only 0.3 mm yr^{-1} higher than their GRACE-based counterparts [Haines et al., 2011], a difference which is commensurate with the uncertainty in ITRF2008 [Collilieux et al., 2014]. Errors in realizing the absolute scale bias carry fewer science consequences than scale instabilities, which can have crucial impacts on the monitoring of global sea level change. The discrepancies in scale bias, however, do reinforce the existence of important open questions about the source of remaining antenna calibration errors.

To lend more insight on the discrepancy between the T/P- and GRACE-based APV estimates for the GPS satellites (Figure 4), it would be worthwhile to take comprehensive measurements of a proxy T/P GPS antenna (e.g., engineering model) in an anechoic chamber. The anechoic values could be compared to the outdoor test range estimates [Young et al., 1993] to probe for potential errors. Efforts to locate such an antenna model have not yet been successful, but one could potentially be manufactured according to the original drawings. Another obvious experiment to improve the LEO-based calibrations would be to roll and pitch one of the GRACE satellites while it actively tracks GPS satellites. The changing relative antenna orientations (transmit versus receiver) would more effectively eliminate singularities that confound simultaneous estimation of the antenna patterns. Such an exercise might be possible before the end of the GRACE mission. Meanwhile, we plan to leverage other suitable LEO missions (e.g., CHAMP) to provide new competing measurements of

the GPS satellite antenna patterns. If approved, the dedicated GRASP mission will offer the best prospects for on-orbit calibration of transmit antennas on GPS and other GNSS satellites [Nerem *et al.*, 2011].

Similar efforts are needed to improve our understanding of the APV patterns of the ground antennas. Characterizing site-specific effects is particularly important. The near-field multipath can systematically alter the intrinsic APV of the antennas [cf. Figure 4 of Elósegui *et al.*, 1995], and failure to account for these effects can induce significant errors in the estimated station height. The notion that near-field effects may not average down globally—impacting the scale of the whole network—should not be discounted. Site-specific APV calibrations can be readily developed using empirical techniques [Hurst and Bar-Sever, 1998]. Characterizing the absolute pattern correctly, however, may first require the use of dedicated calibration systems [e.g., Park *et al.*, 2004; Wübbena *et al.*, 2006] at one or more reference stations in order to compensate for singularities with the network scale.

Better models of the nonconservative (surface) forces on the GPS satellites would also help. Our long-arc POD strategy is highly dynamical, thereby placing a greater burden on the accuracy of the force models. This strategy is designed to stabilize the TRF realizations in the long term but may actually aggravate certain periodic (e.g., draconitic) errors, especially along the spin axis. Recent advances in modeling the GPS satellite surface forces [e.g., Rodriguez-Solano *et al.*, 2014] have shown promise for reducing spurious draconitic errors and should be pursued further.

As demonstrated in the present study using GRACE, inclusion of LEO data in the ground network solutions offers great promise for reducing draconitic errors in realizations of the Earth CM along the spin axis. This result is buttressed by simulations [Kuang *et al.*, 2015], which also underscore the importance of varied low Earth orbits, particularly those with retrograde inclinations to promote faster-changing geometries with respect to the GPS constellation. Routine inclusion in the network solutions of data from a variety of LEO missions likely represents the best future framework for improving the TRF with GNSS.

Finally, realization of the TRF from GPS could clearly benefit from tighter constraints on the GPS satellite clocks [Rebischung *et al.*, 2013]. As newer GNSS satellites are launched with ever-improving frequency standards, this should emerge as an important topic of research.

Appendix A: On the Independence of the Dynamical Models

We have taken significant measures to remove any link between the GPS measurement models—most notably the antenna calibrations—and the fundamental parameters of the TRF as defined by other geodetic techniques (SLR and VLBI). Fingerprints of these techniques, especially SLR, are also found on the background force models used in describing the motions of both the GPS satellites and the low Earth orbiters (GRACE and T/P). Our notion of independence does not contemplate the burden of rederiving—using GPS data alone in the absence of a TRF—these background models. While we treat them in this sense as fundamental, we must also recognize they are neither static nor perfect. We must therefore be alert to any deterioration of the background models that cannot be compensated through the processing of GPS data against the backdrop of a GPS-derived TRF. This appendix addresses the two most important background models, geopotential and solar radiation pressure, and aims to characterize the sensitivity of our results to their uncertainties.

For the geopotential model, the zeroth-degree ($n = 0$) term of the spherical harmonic expansion represents the geocentric gravitation constant (GM). As described in section 2.2, this fundamental constant is inextricably linked in our approach to the recovery of the GPS satellite antenna calibrations from LEO data. The value of GM is thus fixed in our analysis to the IERS standard [Ries *et al.*, 1992], which is derived solely from SLR. The uncertainty of GM , presently estimated at 0.5 ppb [Dunn *et al.*, 1999; Ries and Cheng, 2014], impacts not only the orbital constraint and thus the antenna calibrations (cf. section 2.2) but also the scale of the realized TRF. With GPS, the latter effect is fortunately quite small due to the differential nature of the measurements. In particular, a change of 0.5 ppb in GM imparts a scale error of only 0.03 ppb (0.2 mm at the Earth's surface) to the TRF [Zhu *et al.*, 2003]. This is negligible compared to the scale inconsistencies (few ppb) we observe using different antenna model pairings, and even smaller than the ambitious 1 mm goal for defining the TRF scale [NRC, 2010]. Any future refinements to the value of this fundamental constant would be difficult to perceive in our current TRF realizations.

For the purposes of TRF applications in the foreseeable future, we can also consider GM immutable. Variations in the universal gravitational constant (G)—postulated by Dirac [1937] but as yet unconfirmed—would be

exceedingly small for our application. Using lunar laser ranging, *Williams et al.* [2004] tested the universality of free fall and estimated that \dot{G}/G cannot be significantly different from zero at the 10^{-12} yr^{-1} level. Variations in the Earth's total mass (M)—due mainly to light gases escaping the atmosphere and accretion of cosmic dust—are considered negligible.

The degree 1 ($n = 1$) terms of the static geopotential model represent the 3-D coordinates of the point mass and vanish by definition since the expansion is taken about the CM of the Earth system. Though less relevant to TRF realizations, higher-order terms of the geopotential expansion must also be considered. To describe the motions of the GPS and LEO satellites in our solutions (cf. Tables 3 and 4), we use the GGM02C model [*Tapley et al.*, 2005]. With the exception of degree 2 ($n = 2$) terms, the field is static and derived entirely from GRACE GPS and K band ranging data (for longer wavelengths) and terrestrial gravity data (for shorter wavelengths). While the oblateness (J_2) term and its time derivative are based mainly on multidecadal SLR observations [*Tapley et al.*, 2005; *Nerem et al.*, 1993], GPS data collected in LEO could also be used to provide these estimates [e.g., *Lin et al.*, 2012]. Rates for the degree 2, order 1 terms are set according to the IERS 2003 standards [*McCarthy and Petit*, 2003] and represent long-term motion of the Earth's principal figure axis [e.g., *Cheng et al.*, 2011]. From the perspective of the TRF, these correspond to pure rotations and should have negligible influence on the realization of geocenter and scale in our network-free approach.

The background GPS solar radiation pressure (SRP) model, GSPM13 [*Sibois et al.*, 2014], is based on an empirical approach described by *Bar-Sever and Kuang* [2004], in which the force is represented as a truncated Fourier expansion about the Earth-Satellite-Sun angle. In order to support greater accumulation (and observability) of SRP errors, long integrations of 5 to 10 days are used. The integrated orbit solutions are subsequently fit to "truth" ephemerides by estimating the Fourier series parameters together with epoch states. Results are combined across many years—from 1992 to 2013 in the case of GSPM13—in order to derive SRP models for each GPS satellite block. The truth ephemerides for the GSPM13 model were drawn from the JPL product archive in 2013 and represent the best available, conventional solutions at that time. In particular, they are based on the IGS08 realization of ITRF2008, use the IGS08 conventions for characterizing the antenna phase properties, and apply a prior (2010) version of the GSPM SRP model.

We think future updates of the GSPM models (e.g., to include the future GPS III satellite block) would be uncompromised by the use of alternative selections for the truth solutions (either from a network-free solution or with underpinning from a GPS-defined frame). This remains, however, to be demonstrated. Moreover, questions could be fairly raised about the current results and the potential role of the GSPM13 in communicating some aspects of the SLR geocenter (from ITRF2008) to the GPS realizations via the model parameters [e.g., *Meindl et al.*, 2013]. To address these concerns, we repeat our nominal TRF solution (1997–2013) without explicit modeling of SRP on the GPS satellites. In particular, we reduce the scale coefficient (C_R) from 1 to 10^{-12} , effectively turning off the photon flux that drives the background model and the accelerations linked to it. In lieu of the SRP coefficient (C_R) and Y bias (cf. Table 4), we estimate—as bias parameters per 9 day solution—three empirical accelerations in solar (UVW) coordinates as viewed from the spacecraft. (U points away from the Sun, V points along the cross product between the U and geocenter directions, and W completes the right-hand system.) The accelerations are treated as constants scaled by a shadow factor, which ranges from 0 to 1 as the satellite passes from eclipse to full sun.

We refer to this strategy as "photon free" and note that the overall approach is similar, though not identical, to that underlying the current Center for Orbit Determination in Europe (CODE) model [*Beutler et al.*, 1994; *Springer et al.*, 1999]. The CODE model provides for the estimation of a set of (5) empirical accelerations in the same solar coordinate system and, as currently practiced, does not use a background SRP model. The absence of any background model is compensated by the introduction of empirical accelerations in a coordinate system consistent with the Sun-Probe geometry.

For our controlled test spanning 1997–2013, the results from the photon-free case testify to both the overall resilience and remaining weaknesses of the GPS-based TRF. The scale (2005.0) and scale rate are altered insignificantly—by 0.3 mm and $+0.04 \text{ mm yr}^{-1}$, respectively—from the nominal case. Equally promising results are obtained for the origin along the equatorial plane, with deviations of only 0.1 mm and 0.1 mm yr^{-1} . Only the origin along the spin (Z) axis shows important changes: 6 mm and 0.5 mm yr^{-1} for bias (2005.0) and rate, respectively. These changes, however, remain consistent with expected errors in contemporary realizations of the TRF [*Collilieux et al.*, 2014].

Table A1. Comparison of GPS-Based TRF With ITRF2008/IGb08: Nominal Versus "Photon Free"^a

Fit Parameter	Scale	X	Y	Z
ΔBias (2005.0, mm)	7.3/7.5	5.4/5.4	3.8/3.8	3.9/9.6
ΔRate (mm yr ⁻¹)	0.2/0.2	0.3/0.4	-0.0/-0.1	0.3/0.8
Annual amplitude (mm)	1.0/1.0	0.8/0.1	3.6/4.2	4.6/14.1
Annual phase (day of year)	77/75	286/50	328/326	282/17
Postfit residual (mm)	1.6/1.6	4.6/4.7	5.1/5.1	11.1/14.9

^aEach pair of numbers in the table represents a nominal/photon-free result.

Provided in Table A1 are statistics on the comparisons of the two GPS-based TRF solutions (nominal and photon free) to the IGb08 realization of ITRF2008. As expected, the largest discrepancy is observed for the annual geocenter motion along the spin axis, providing further support for our conclusion that this periodic effect is not well determined by GPS in the Z direction. More relevant to the frame definition, the photon-free approach increases the discrepancy in the Z rate from 0.3 to 0.8 mm yr⁻¹. While the latter figure may be slightly significant, it is not an unexpected outcome when comparing two independent, state-of-the-art frames stable at the 0.5 mm yr⁻¹ level. Based on the weekly repeatabilities of the solutions, however, there is reason to believe that the photon-free solution is inferior. *Sibthorpe et al. [2011]* provide further evidence of the benefits of the GSPM background model. Despite the fact that the photon-free approach yields competitive results for long-term realization of the TRF, a GSPM-based approach remains our preference, and we think that future versions of the GSPM model can be developed without recourse to the ITRF.

Acknowledgments

The work described in this paper was performed at the Jet Propulsion Laboratory, California Institute of Technology, under a contract with the National Aeronautics and Space Administration. We thank our JPL colleagues Charles Dunn and Larry Young for providing the calibrations from the JPL outdoor test range for both the TOPEX/Poseidon and TurboRogue antennas; George Purcell for providing the anechoic calibrations for the GRACE antennas, and Sung Byun for producing the simulated multipath estimates for GRACE. We are grateful for fruitful discussions with our JPL collaborators, especially Da Kuang, Mike Heflin, and Xiaoping Wu, the latter of whom kindly provided estimates of annual geocenter motion from his inverse method. We also thank Gerhard Wübbena and Martin Schmitz of geo++ for providing data from the robotic field calibration of the GPS Block IIA antenna assembly. We are grateful to Zuheir Altamimi and an anonymous reviewer for their valuable comments on this manuscript. The GPS tracking data from both ground stations and low Earth orbiters are available from <http://cds.gsfc.nasa.gov>, while the JPL products for the GPS constellation are available at ftp://sideshow.jpl.nasa.gov/pub/JPL_GPS_Products. High-level data products underlying all the plots in the paper are available on request from author B.H.

References

- Altamimi, Z., and X. Collilieux (2009), IGS contribution to the ITRF, *J. Geod.*, 83(3–4), 375–383, doi:10.1007/s00190-008-0294.
- Altamimi, Z., X. Collilieux, and L. Métivier (2011), ITRF2008: An improved solution of the international terrestrial reference frame, *J. Geod.*, 85(8), 457–473, doi:10.1007/s00190-011-0444-4.
- Anderle, R. J. (1978), Application of the Global Positioning System to determination of tectonic plate movements and crustal deformations, in *Proceedings of the 9th Geodesy/Solid Earth and Ocean Physics (GEOP) Research Conference, An International Symposium on the Applications of Geodesy to Geodynamics*, edited by I. I. Mueller, IAG/IUGG, and COSPAR, Columbus, U.S.A., October, Department of Geodetic Science Report 280, The Ohio State Univ., Columbus, pp. 53–57.
- Aparicio, M., P. Brodie, L. Doyle, J. Rajan, and P. Torrione (1996), GPS satellite and payload, in *Global Positioning System: Theory and Applications I*, *Prog. Astronaut. Aero.*, vol. 163, edited by B. Parkinson and J. Spilker Jr., pp. 209–244, AIAA, Washington, D.C.
- Argus, D. F. (2012), Uncertainty in the velocity between the mass center and surface of Earth, *J. Geophys. Res.*, 117, B10405, doi:10.1029/2012JB009196.
- Berger, C., R. Biancale, M. Ill, and F. Barlier (1998), Improvement of the empirical thermospheric model DTM: DTM94—A comparative review of various temporal variations and prospects in space geodesy applications, *J. Geod.*, 72(3), 161–178, doi:10.1007/s001900050158.
- Bar-Sever, Y., and D. Kuang (2004), New empirically derived solar radiation pressure model for Global Positioning System satellites, *Interplanet. Network Prog. Rep.* 42–159, Jet Propul. Lab., Calif., pp. 1–11. [Available at http://ipnpr.jpl.nasa.gov/progress_report/42-159/159.pdf]
- Bar-Sever, Y. (1996), A new yaw model for GPS attitude, *J. Geod.*, 70, 714–723.
- Bar-Sever, Y. (1998), Estimation of the GPS transmit phase center offset (abstract), *Eos Trans. AGU*, 79(45), 183.
- Bertiger, W. I., et al. (1994), GPS precise tracking of TOPEX/POSEIDON: Results and implications, *J. Geophys. Res.*, 99(C12), 24,449–24,464, doi:10.1029/94JC01171.
- Bettadpur, S. (2012), GRACE 327-720 (CSR-GR-03-02). Gravity Recovery and Climate Experiment, product specification document, Rev 4.6, Center for Space Research, Univ. of Texas, Austin.
- Beckley, B., F. Lemoine, S. Luthcke, R. Ray, and N. P. Zelensky (2007), A reassessment of global and regional mean sea level trends from TOPEX and Jason-1 altimetry based on revised reference frame and orbits, *Geophys. Res. Lett.*, L14608, doi:10.1029/2007GL030002.
- Beutler, G., E. Brockmann, W. Gurtner, U. Hugentobler, L. Mervart, and M. Rothacher (1994), Extended orbit modeling techniques at the code processing center of the International GPS Service for Geodynamics (IGS): Theory and initial results, *Manuscr. Geodaet.*, 19, 367–386.
- Beutler, G., M. Rothacher, S. Schaer, T. A. Springer, J. Kouba, and R. E. Neilan (1999), The International GPS Service (IGS): An interdisciplinary service in support of Earth sciences, *Adv. Space Res.*, 23(4), 631–653, doi:10.1016/S0273-1177(99)00160-X.
- Blewitt, G., M. B. Heflin, F. H. Webb, U. J. Lindqwister, and R. P. Malla (1992), Global coordinates with centimeter accuracy in the international terrestrial reference frame using GPS, *Geophys. Res. Lett.*, 19(9), 853–856, doi:10.1029/92GL00775.
- Blewitt, G., D. Lavallée, P. Clarke, and K. Nurudinov (2001), A new global mode of Earth deformation: Seasonal cycle detected, *Science*, 294(5550), 2342–2345.
- Blewitt, G., et al. (2010), Geodetic observations and global reference frame contributions to understanding sea-level rise and variability, in *Understanding Sea-Level Rise and Variability*, edited by J. Church, pp. 256–284, Wiley-Blackwell, Oxford, U.K.
- Boehm, J., A. E. Niell, P. Tregoning, and H. Schuh (2006), Global mapping functions (GMF): A new empirical mapping function based on numerical weather model data, *Geophys. Res. Lett.*, 33, L07304, doi:10.1029/2005GL025545.
- Boehm, J., R. Heinkelmann, and H. Schuh (2007), Short note: A global model of pressure and temperature for geodetic applications, *J. Geod.*, 81, 679–683, doi:10.1007/s00190-007-0135-3.
- Born, G. H., B. D. Tapley, J. C. Ries, and R. Stewart (1986), Accurate measurement of mean sea level changes by altimetric satellites, *J. Geophys. Res.*, 91(C10), 11,755–11,782.

- Bruinsma, S., G. Thuillier, and F. Barlier (2003), The DTM-2000 empirical thermosphere model with new data assimilation and constraints at lower boundary: Accuracy and properties, *J. Atmos. Sol. Terr. Phys.*, 65(9), 1053–1070, doi:10.1016/S1364-6826(03)00137-8.
- Byun, S., G. Hajj, and L. Young (2002), Development and application of GPS signal multipath simulator, *Radio Sci.*, 37(6), 10–1–10–23, doi:10.1029/2001RS002549.
- Cheng, M., J. C. Ries, and B. D. Tapley (2011), Variations of the Earth's figure axis from satellite laser ranging and GRACE, *J. Geophys. Res.*, 116, B01409, doi:10.1029/2010JB00850.
- Cardellach, E., P. Elósegui, and J. L. Davis (2007), Global distortion of GPS networks associated with satellite antenna model errors, *J. Geophys. Res.*, 112, B07405, doi:10.1029/2006JB004675.
- Collilieux, X., and G. Wöppelmann (2011), Global sea-level rise and its relation to the terrestrial reference frame, *J. Geod.*, 85(1), 9–22, doi:10.1007/s00190-010-0412-4.
- Collilieux, X., L. Métivier, Z. Altamimi, T. van Dam, and J. Ray (2011), Quality assessment of GPS reprocessed terrestrial reference frame, *GPS Solut.*, 15, 219–231, doi:10.1007/s10291-010-0184-6.
- Collilieux, X., et al. (2014), External evaluation of the ITRF2008: Report of the task force of the IAG sub-commission 1.2, in *Earth on the Edge: Science for a Sustainable Planet, Intl. Assoc. of Geodesy Symposia*, vol. 139, edited by C. Rizos and P. Willis, pp. 197–202, Springer, Berlin., doi:10.1007/978-3-642-37222-3_25.
- Counselman, C., and I. Shapiro (1979), Miniature interferometer terminals for Earth surveying, *Bull. Geod.*, 53, 139–163.
- Desai, S., W. Bertiger, B. Haines, D. Kuang, C. Lane, A. Sibois, F. Webb, and J. Weiss (2008), Defining the terrestrial reference frame from GPS: Results from a JPL reanalysis, Abstract G32A-03 presented at 2008 Fall Meeting, AGU, San Francisco, Calif., 15–19 Dec.
- Desai, S., W. Bertiger, B. Haines, N. Harvey, C. Selle, A. Sibthorpe, and J. Weiss (2011), Results from the reanalysis of global GPS data in the IGS08 reference frame. Abstract G53B-0904 presented at 2011 Fall Meeting, AGU, San Francisco, Calif., 5–9 Dec.
- Desai, S., W. Bertiger, M. Garcia-Fernandez, B. Haines, D. Murphy, C. Selle, A. Sibois, A. Sibthorpe, and J. P. Weiss (2014), Status and plans at the JPL IGS analysis center, in *Intl. GNSS Service 2014 Workshop Compendium, Ed. IGS Central Bureau*, p. 53., Jet Propul. Lab., Calif. Inst. of Technol., Pasadena, Calif. [Available at <http://www.igs.org/workshop/posters>.]
- Dilssner, F. (2010), GPS IIF-1 Satellite Antenna Phase Center and Attitude Modeling. Inside GNSS, 59–64, September 2010.
- Dirac, P. A. M. (1937), The cosmological constants, *Nature*, 139(3512), 323—323.
- Dong, D., T. Yunck, and M. Heflin (2003), Origin of the international terrestrial reference frame, *J. Geophys. Res.*, 108(B4), 2200, doi:10.1029/2002JB002035.
- Dunn, P., M. Torrence, R. Kolenkiewicz, and D. Smith (1999), Earth scale defined by modern satellite ranging observations, *Geophys. Res. Lett.*, 26(10), 1489–1492.
- Eanes, R., and S. Bettadpur (1996), The CSR3.0 global ocean tide model: Diurnal and semi-diurnal ocean tides from TOPEX/POSEIDON altimetry, *Tech. Rep. CRS-TM-96-05*, Cent. for Space Res., Univ. of Texas, Austin, Texas.
- Elósegui, R., J. L. Davis, R. T. K. Jaldehag, J. M. Johansson, A. E. Niell, and I. I. Shapiro (1995), Geodesy using the global positioning system: The effects of signal scatter on estimates of site position, *J. Geophys. Res.*, 100(B7), 9921–9934.
- Even-Tzur, G., and D. Shaked (2008), GPS antenna height and its influence on pseudorange multipath, Integrating Generations, FIG Working Week 2008 Stockholm, Sweden 14–19 June 2008. [Available at https://www.fig.net/pub/fig2008/papers/ts05g/ts05g_03_eventzur_shaked_2816.pdf.]
- Fu, L.-L., and B. Haines (2013), The challenges in long-term altimetry calibration for addressing the problem of global sea-level change, *Adv. Space Res.*, 51, 1284–1300, doi:10.1016/j.asr.2012.06.005.
- Gambis, D., and B. Luzum (2011), Earth rotation monitoring, UT1 determination and prediction, *Metrologia*, 48, S16–S170, doi:10.1088/0026-1394/48/4/S06.
- García-Fernandez, M., S. D. Desai, M. D. Butala, and A. Komjathy (2013), Evaluation of different approaches to modeling the second-order ionospheric delay on GPS measurements, *J. Geophys. Res. Space Physics*, 118, 7864–7873, doi:10.1002/2013JA019356.
- Ge, M., G. Gent, D. Dick, F. P. Zhang, and C. Reigber (2005), Impact of GPS satellite antenna offsets on scale changes in global network solutions, *Geophys. Res. Lett.*, 32, L06310, doi:10.1029/2004GL022224.
- Griffiths, J., and J. R. Ray (2009), On the precision and accuracy of IGS orbits, *J. Geod.*, 83, 277–287, doi:10.1007/s00190-008-0237-6.
- Haines, B., Y. Bar-Sever, W. Bertiger, S. Desai, and P. Willis (2004), One-centimeter orbit determination for Jason-1: New GPS-based strategies, *Mar. Geod.*, 27(1–2), 299–318.
- Haines, B., Y. Bar-Sever, W. Bertiger, S. Byun, S. Desai, and G. Hajj (2005), GPS antenna phase center variations: New perspectives from the GRACE Mission. [Available at http://wwwrc.obs-azur.fr/ftp/gmc/swt/Bruce/Haines_IAG.ppt.]
- Haines, B., Y. Bar-Sever, W. Bertiger, S. Byun, S. Desai, and G. Hajj (2006), Using GRACE as an orbiting fiducial laboratory for GPS, *Eos Trans. AGU*, 87(52), Fall Meet. Suppl., Abstract G11B–07.
- Haines, B., Y. Bar-Sever, W. Bertiger, S. Desai, S. Owen, A. Sibois, and F. Webb (2007), GRACE-based estimates of GPS satellite antenna phase variations: Impact on determining the scale of the terrestrial reference frame, *Eos Trans. AGU*, 88(52), Fall Meet. Suppl., Abstract G42A–0.
- Haines, B., Y. Bar-Sever, W. Bertiger, S. Desai, N. Harvey, and J. Weiss (2010), Improved models of GPS satellite antenna phase- and group-delay variations using data from low-Earth orbiters, *Eos Trans. AGU*, 91(26), Meet. Am. Suppl., Abstract G54A–05. [Available at http://acc.igs.org/antennas/sat-ant-offsets_jpl_AGU10.pdf.]
- Haines, B., Y. Bar-Sever, W. Bertiger, S. Desai, N. Harvey, and J. Weiss (2011), A GPS-based terrestrial reference frame from a combination of terrestrial and orbiter data, Abstract G53A–0880 presented at 2011 Fall Meeting, AGU, San Francisco, Calif. [Available at http://acc.igs.org/trf/gps+leo-frame_agu11poster.pdf.]
- Hajj, G. (1989), The multipath simulator: A tool toward controlling multipath. [Available at <http://oai.dtic.mil/oai/oai?verb=getRecord&metadataPrefix=html&identifier=ADA219978>.]
- Heflin, M., et al. (1992), Global geodesy using GPS without fiducial sites, *Geophys. Res. Lett.*, 19(2), 131–134.
- Heflin, M., D. Argus, D. Jefferson, F. Webb, and J. Zumberge (2002), Comparison of a GPS-defined global reference frame with ITRF2000, *GPS Solut.*, 6, 72–75.
- Hurst, K. J., and Y. Bar-Sever (1998), Site specific phase center maps for GPS stations, *Eos Trans. AGU*, 79(45), Fall Meet. Suppl., Abstract G71B–13.
- Jäggi, A., F. Dilssner, R. Schmid, R. Dach, T. Springer, H. Bock, P. Steigenberger, Y. Andres, and W. Enderle (2013), Extension of the GPS satellite antenna patterns to nadir angles beyond 14°, paper presented at IGS workshop 2012, Institute for Astronomical and Physical Geodesy, Technische Universität München, 23–27, 2012, July, Olzstyn, Poland. [Available at <http://www.igs.org/assets/pdf/Poland%202012%20-%20P09%20Dach%20PR14.pdf>.]
- Kang, Z., B. Tapley, J. Chen, J. Ries, and S. Bettadpur (2009), Geocenter variations derived from GPS tracking of the GRACE satellites, *J. Geod.*, 83, 895–901.

- Knoche, P. C. (1989), Earth radiation pressure effects on satellites, CSR-89-1, Univ. of Texas, Austin. [Available at <ftp://ftp.csr.utexas.edu/pub/reports/CSR-89-1.pdf>.]
- Kuang, D., B. E. Schutz, and M. M. Watkins (1996), On the structure of geometric positioning information in GPS measurements, *J. Geod.*, **71**, 35–43.
- Kuang, D., Y. Bar-Sever, and B. . Haines (2015), Analysis of orbital configurations for geocenter determination with GPS and low-Earth orbiters, *J. Geod.*, **89**(5), 471–481, doi:10.1007/s00190-015-0792-6.
- Lavallée, D., T. van Dam, G. Blewitt, and P. Clarke (2006), Geocenter motions from GPS: A unified observation model, *J. Geophys. Res.*, **111**, B05405, doi:10.1029/2005JB003784.
- Love, A. W. (1984), *Phase Center Location and Group Delay in the GPS L-Band and W-Sensor Antenna*, Internal Document, Rockwell International, Seal Beach, Calif.
- Lin, T., C. Hwang, T.-P. Tseng, and B. Chao (2012), Low-degree gravity change from GPS data of COSMIC and GRACE satellite missions, *J. Geodyn.*, **53**, 34–42, doi:10.1016/j.jog.2011.08.004.
- Lyard, F., F. Lefevre, T. Letellier, and O. Francis (2006), Modelling the global ocean tides: Modern insights from FES2004, *Ocean Dyn.*, **56**(5–6), 394–315, doi:10.1007/s10236-006-0086-x.
- MacDoran, P. (1979), Satellite emission radio interferometric Earth surveying: SERIES—GPS geodetic system, *Bull. Geod.*, **53**, 117–138.
- Mader, G. (1999), GPS antenna calibration at the National Geodetic Survey, *GPS Solut.*, **3**(1), 50–58.
- Mader, G., and F. Czopek (2001), Calibrating the L1 and L2 phase centers of a Block IIA antenna. paper presented at 14th International Technical Meeting of the Satellite Division of The Institute of Navigation (ION GPS 2001), Salt Lake City, UT, 11–14 Sept., 2001.
- Mader, G., and F. Czopek (2002), The Block IIA satellite: Calibrating antenna phase centers, *GPS World*, **13**(5), 40–46.
- Malla, R. P., and S.-C. Wu (1989), GPS inferred geocentric reference frame for satellite positioning and navigation, *Bull. Geod.*, **63**(3), 263–279, doi:10.1007/BF02520476.
- Malla, R., S. Wu, and S. Lichten (1993a), Geocenter location and variations in Earth orientation using global positioning system measurements, *J. Geophys. Res.*, **98**(B3), 4611–4617.
- Malla, R., S. Wu, S. Lichten, and Y. Vigue (1993b), Breaking the ΔZ barrier in geocenter estimation, *Eos Trans. AGU*, **74**(43), Fall Meet. Suppl., Abstract G21A–11.
- Malys, S., J. Seago, N. Pavlis, P. K. Seidelmann, and G. Kaplan (2015), Why the Greenwich meridian moved, *J. Geodesy*, doi:10.1007/s00190-015-0844-y.
- Marshall, J. A., and S. Luthcke (1994), Modeling radiation forces acting on TOPEX/Poseidon for precision orbit determination, *J. Spacecraft Rockets*, **31**(1), 99–105.
- McCarthy, D., and G. Petit (Eds.) (2003), IERS Conventions 2003, *IERS Techn. Note 32*, Frankfurt am Main: Verlag des Bundesamts für Kartographie und Geodäsie. 127 pp., paperback, (print version).
- Meindl, M., G. Beutler, D. Thaller, R. Dach, and A. Jäggi (2013), Geocenter coordinates estimated from GNSS data as viewed by perturbation theory, *Adv. Space Res.*, **51**(7), 1047–1064, doi:10.1016/j.asr.2012.10.026.
- Ménard, Y., L.-L. Fu, P. Escudier, F. Parisot, J. Perbos, P. Vincent, S. Desai, B. Haines, and G. Kunstmann (2004), The Jason-1 mission, *Mar. Geod.*, **26**(3–4), 131–146.
- Merkowitz, S., et al. (2012), Next generation NASA initiative for space geodesy. Abstract G52B-04 presented at 2012 Fall Meeting, AGU, San Francisco, Calif., 3–7 Dec.
- Morel, L., and P. Willis (2005), Terrestrial reference frame effects on global sea level rise determination from TOPEX/Poseidon altimetric data, *Adv. Space Res.*, **36**, 358–368, doi:10.1016/j.asr.2005.05.113.
- Nerem, S., B. F. Chao, A. Y. Yu, J. C. Chan, S. M. Klosko, N. K. Pavlis, and R. G. Williamson (1993), Temporal variations of the Earth's gravitational field from satellite laser ranging to Lageos, *J. Geophys. Res.*, **20**(7), 595–598.
- Nerem, S., et al. (2011), The Geodetic Reference Antenna in Space (GRASP)—A Mission to Enhance the Terrestrial Reference Frame, Abstract G51B-04 presented at 2011 Fall Meeting, AGU, San Francisco, Calif.
- NRC (National Research Council) (2010), *Precise Geodetic Infrastructure: National Requirements for a Shared Resource*, Natl. Academies Press, Washington, D. C. [Available at <http://www.nap.edu>.]
- Park, K.-D., P. Elósegui, J. L. Davis, P. O. J. Jarlemark, B. E. Corey, A. E. Niell, J. E. Normandeau, C. E. Meertens, and V. A. Andreatta (2004), Development of an antenna and multipath calibration system for global positioning system sites, *Radio Sci.*, **39**, RS5002, doi:10.1029/2003RS002999.
- Petit, G., and B. Luzum (Eds.) (2010), IERS Conventions 2010, *IERS Tech. Note 36*, Verlag des Bundesamts für Kartographie und Geodäsie. Frankfurt am Main, 179 pp.
- Plag, H.-P., and M. Pearlman (Eds.) (2009), *The Global Geodetic Observing System: Meeting the Requirements of a Global Society on a Changing Planet in 2020*, Springer, Berlin.
- Purcell, G. (1999a), Analysis of the Jason antenna pattern. revised, JPL Internal Document, March 24, 1999.
- Purcell, G. (1999b), Further analysis of measurements of Jason antenna patterns. JPL Internal Document, September 1, 1999.
- Ray, J., D. Dong, and Z. Altamimi (2004), IGS reference frames: Status and future improvements, *GPS Solut.*, **8**, 251–266, doi:10.1007/s10291-004-0110-x.
- Ray, J., Z. Altamimi, X. Collilieux, and T. van Dam (2008), Anomalous harmonics in the spectra of GPS position estimates, *GPS Solut.*, **12**, 5–64, doi:10.1007/s10291-007-0067-7.
- Rebischung, P., J. Griffiths, J. Ray, R. Schmid, X. Collilieux, and B. Garayt (2012), IGS08: The IGS realization of ITRF2008, *GPS Solut.*, **16**(4), 483–494, doi:10.1007/s10291-011-0248-2.
- Rebischung, P., Z. Altamimi, and T. Springer (2013), A collinearity diagnosis of the GNSS geocenter determination, *J. Geod.*, **88**, 65–85, doi:10.1007/s00190-013-0669-5.
- Ries, J. C., and M. K. Cheng (2014), Satellite laser ranging applications for gravity field determination, paper presented at 19th International Workshop of Laser Ranging, Annapolis, Maryland, 27–31 Oct. 2014. [Available at http://cddis.gsfc.nasa.gov/lw19/docs/2014/Papers/3117_Ries_paper.pdf.]
- Ries, J. C., R. J. Eanes, C. K. Shum, and M. M. Watkins (1992), Progress in the determination of the gravitational coefficient of the Earth, *Geophys. Res. Lett.*, **19**(6), 529–531.
- Rodriguez-Solano, C. J., U. Hugentobler, P. Steigenberger, M. Bloßfeld, and A. Fritsche (2014), Reducing the draconitic errors in GNSS geodetic products, *J. Geod.*, **88**(6), 559–574, doi:10.1007/s00190-014-0704-1.
- Rülke, A., R. Dietrich, M. Fritsche, M. Rothacher, and P. Steigenberger (2008), Realization of the terrestrial references system by a reprocessed global GPS network, *J. Geophys. Res.*, **113**, B08403, doi:10.1029/2007JB005231.
- Schmid, R. (2012), The IGS antenna working group, in *IGS Technical Report 2012*, edited by M. Meindl, R. Dach, and Y. Jean, pp. 141–147, IGS Cent. Bureau, Jet Propul. Lab., Pasadena, Calif.

- Schmid, R., and M. Rothacher (2003), Estimation of elevation-dependent satellite antenna phase center variations of GPS satellites, *J. Geod.*, 77(7–8), 440–446.
- Schmid, R., M. Rothacher, D. Thaller, and P. Steigenberger (2005), Absolute phase center corrections of satellite and receiver antennas: Impact on global GPS solutions and estimation of azimuthal phase center variations of the satellite antenna, *GPS Solut.*, 9, 283–293, doi:10.1007/s10291-005-0134-x.
- Sibois, A. (2011), GPS-based sub-hourly polar motion estimates: Strategies and applications, ProQuest Dissertations and Theses, PhD thesis, Univ. of Colorado, Boulder, Colo. AAT 3489556, ISBN: 9781267089052; Source: Dissertation Abstracts International, Volume: 73-04, Section: B, 293 pp.
- Sibois, A., C. Selle, S. Desai, A. Sibthorpe, and J. Weiss (2014), An updated empirical model for solar radiation pressure forces acting on GPS satellites (abstract), Intl. GNSS Service Workshop, Pasadena. [Available at <http://beta.igs.org/workshop/posters>.]
- Sibthorpe, A., W. Bertiger, S. Desai, B. Haines, N. Harvey, and J. Weiss (2011), An evaluation of solar radiation pressure strategies for the GPS constellation, *J. Geod.*, 85(8), 505–517, doi:10.1007/s00190-011-0450-6.
- Springer, T. (2000), Common interests of the IGS and the IVS, in *Proceedings of International VLBI Service for Geodesy and Astrometry 2000 General Meeting*, edited by N. R. Vandenberghm and K. D. Bauer, pp. 296–305, NASA, Koettzing, Germany.
- Springer, T., and F. Diltsner (2009), SVN49 and other GPS anomalies: Elevation dependent pseudorange errors in Block IIRs and IIR-Ms. Inside GNSS, 32–36 July/August.
- Springer, T., G. Beutler, and M. Rothacher (1999), Improving the orbit estimates of GPS satellites, *J. Geod.*, 73(3), 147–157.
- Standish, M. (1998), JPL Planetary and Lunar Ephemerides, DE405/LE405" JPL Interoffice Memorandum 312.F–98-048. [Available at <http://iau-comm4.jpl.nasa.gov/de405iom/de405iom.pdf>.]
- Steigenberger, P., M. Rothacher, M. Fritzsche, A. Rülke, and R. Dietrich (2009), Quality of reprocessed GPS satellite orbits, *J. Geod.*, 83, 241–248, doi:10.1007/s00190-008-0228-7.
- Tapley, B. D., S. Bettadpur, M. Watkins, and C. Reigber (2004), The gravity recovery and climate experiment: Mission overview and early results, *Geophys. Res. Lett.*, 31, L06619, doi:10.1029/2003GL019285.
- Tapley, B. D., et al. (2005), GGM02—An improved earth gravity field model from GRACE, *J. Geod.*, 79, 467–478, doi:10.1007/s00190-005-0480-z.
- Tetewsky, A., et al. (2014), Inter-signal correction sensitivity analysis: Assessing SV aperture dependent delays and ground control approximations on modernized GPS dual frequency navigation. Inst. of Navigation 2014 Joint Navigation Conference, Orlando, 16–19 June.
- Tranquilla, J. M., and B. G. Colpitts (1989), Development of a class of antennas for space-based Navstar GPS applications, in *Intl. Conference on Antennas and Propagation (ICAP 89), 6th, Coventry, England, Apr. 4–7, 1989, Proceedings. Part 1 (A90-27776 11-32)*, pp. 65–69, Inst. of Electr. Eng., London, England and Piscataway, N. J. [Available at <http://ieeexplore.ieee.org/stamp/stamp.jsp?tp=&rnumber=29709>.]
- Tranquilla, J. M., J. P. Carr, and H. M. Al-Rizzo (1994), Analysis of a choke ring ground plane for multipath control in Global Positioning System (GPS) applications, *IEEE Trans. Antennas Propag.*, 42(7), 905–911.
- Vigue, Y., S. M. Lichten, G. Blewitt, M. B. Heftin, and R. P. Malla (1992), Precise determination of Earth's center of mass using measurements from the Global Positioning System, *Geophys. Res. Lett.*, 19, 1487–1490, doi:10.1029/92GL01575.
- Weiss, J., W. Bertiger, S. Desai, B. Haines, and A. Sibois (2013), Two decade terrestrial reference frame time series from GPS (abstract), IAG Scientific Assembly, Potsdam. [Available at http://www.iag2013.org/IAG_2013/Publication_files/abstracts_iag_2013_2808.pdf.]
- Williams, J., S. G. Turyshev, and D. H. Boggs (2004), Progress in Lunar Laser Ranging Tests of Relativistic Gravity, *Phys. Rev. Lett.*, 93, 261101, doi:10.1103/PhysRevLett.93.261101.
- Wu, X., X. Collilieux, Z. Altamimi, B. L. A. Vermeersen, R. S. Gross, and I. Fukumori (2011), Accuracy of The International Terrestrial Reference Frame origin and Earth expansion, *Geophys. Res. Lett.*, 38, L13304, doi:10.1029/2011GL047450.
- Wu, X., J. Ray, and T. van Dam (2012), Geocenter motion and its geodetic and geophysical implications, *J. Geodyn.*, 58, 44–61, doi:10.1016/j.jog.2012.01.007.
- Wu, X., C. Abbondanza, Z. Altamimi, T. M. Chin, X. Collilieux, R. S. Gross, M. B. Heflin, Y. Jiang, and J. W. Parker (2013), Geocenter motion and degree-1 surface mass variations—Reconciling results from direct SLR determination and inverse estimation, GRACE science team meeting, Potsdam, Germany. [Available at <http://www.csr.utexas.edu/grace/GSTM/b1.html>.]
- Wübbena, G., M. Schmitz, F. Böder, V. Menge, and G. Seiber (2000), GPS automated absolute field calibration of GPS antennas in real-time. paper presented at 13th International Technical Meeting of the Satellite Division of The Institute of Navigation (ION GPS 2000), Salt Lake City, UT, 19–22 Sept. 2000.
- Wübbena, G., M. Schmitz, and G. Boettcher (2006), Near-field effects on GNSS sites: Analysis using absolute robot calibrations and procedures to determine corrections, paper presented at IGS Workshop 2006 Perspectives and Visions for 2010 and beyond, ESOC, Darmstadt, Germany, 8–12 May.
- Wübbena, G., M. Schmitz, F. Menge, and F. Czopek (2007), GPS Block II/IIA Satellite antenna testing using the automated absolute field calibration with robot, paper presented at 20th International Technical Meeting of the Satellite Division of The Institute of Navigation (ION GNSS 2007), Fort Worth Convention Center, Fort Worth, Texas, 25–28 Sept. 2007.
- Young, L., R. Neilan, and R. Bletzacker (1985), GPS satellite multipath: An experimental investigation. paper presented at First International Symposium on Precise Positioning with the Global Positioning System, Rockville, Maryland, 15–19 April, 1985.
- Young, L., T. Meehan, D. Spitzmesser, and J. Tranquilla (1988), GPS antenna selection: Preliminary range and field test results. paper presented at International Symposium on Antenna Technology and Applied Electromagnetics, Can. Space Agency, Winnipeg, Manit., Canada, 9–12 Aug. 1988.
- Young, L., T. Munson, C. Dunn, and E. S. Davis (1993), GPS precision orbit determination: Measured receiver performance, JPL Technical Document, 93–1616. [Available at <http://trs-new.jpl.nasa.gov/dspace/bitstream/2014/35887/1/93-1616.pdf>.]
- Zhu, S., F.-H. Yo, Massmann, Y., and C. Reigber (2003), Satellite antenna phase center offsets and scale errors in GPS solutions, *J. Geod.*, 76, 668–672.
- Ziebart, M., S. Adya, A. Sibthorpe, S. Edwards, and P. Cross (2005), Combined radiation pressure and thermal modeling of complex satellites: Algorithms and on-orbit tests, *Adv. Space Res.*, 36, 424–430, doi:10.1016/j.asr.2.
- Zumberge, J., R. Neilan, and I. Mueller (1994), Position paper 1: Densification of the IGS global network, in *IGS Workshop Proceedings: Densification of the IERS Terrestrial Reference Frame Through Regional GPS Networks*, edited by J. F. Zumberge and R. Liu, pp. 95–11, JPL Publ., Pasadena. [Available at http://igscb.jpl.nasa.gov/igscb/resource/pubs/zumberge_94a.pdf.]